REPORT No. 53

AN INVESTIGATION OF CAVITATING INDUCERS FOR TURBOPUMPS

PHILIP J. MULLAN

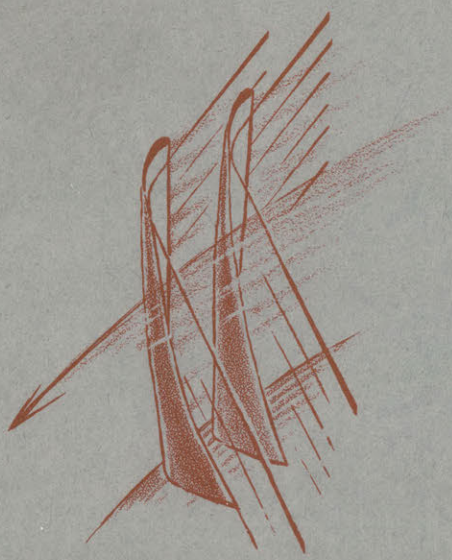

May, 1959

GAS TURBINE LABORATORY
MASSACHUSETTS INSTITUTE OF TECHNOLOGY
CAMBRIDGE · 39 · MASSACHUSETTS

AN INVESTIGATION OF CAVITATING INDUCERS FOR TURBOPUMPS

by

PHILIP J. MULLAN

Under the sponsorship of:

General Electric Company
Westinghouse Electric Corporation
Allison Division of the General Motors Corporation

Gas Turbine Laboratory
Report Number 53

May 1959

Massachusetts Institute of Technology

TABLE OF CONTENTS

ABSTRACT

The experimental performance of two axial inducers is presented. One of the designs is analytical and includes radial equilibrium considerations. The other is a simple helix, with a constant pitch angle. The performance data consists of two parts; conventional non-cavitating pump performance, and performance with cavitation. High speed pictures of the cavitation formations were taken.

ACKNOWLEDGEMENTS

I should like to express my sincere gratitude to Professor E. S. Taylor, Director of the Gas Turbine Laboratory and Professor A. H. Stenning, both of whom initiated this work and provided continual advice and encouragement throughout.

Professor Y. Senoo made many valuable suggestions which helped move this investigation in a forward direction.

Also, I should like to thank G. Miskolczy who designed much of the test section, P. Wassmouth who did the excellent machining, and G. Falla who did the high-speed photography. The other members of the Gas Turbine Laboratory were always ready and willing to help.

Natalie Appleton did the typing.

LIST OF SYMBOLS

A	Annular area ($ft.^2$)
D	Diameter (ft.)
C	Coefficient, velocity component (fps)
H	Head (ft.)
U	Velocity of inducer (fps)
T	Torque
K	Cavitation Number (Prandtl)
W	Relative velocity (fps)
N	Rotational speed (rpm)
Q	Flow rate (cfs)
R	Radius (ft.)
r	Hub-tip ratio
ρ	Density (lb/ft^2)
g	Proportionality constant in Newton's law
SSS	Suction specific speed
ψ	Head coefficient
τ	Torque coefficient
β	Relative exit angle
α	Absolute exit angle (measured from axial direction)

SUBSCRIPTS

v	Vapor pressure
t	Tip
h	Hub
θ	Tangential direction
x	Axial direction
1, 3	Stations (Fig. 1)
s	Suction

LIST OF FIGURES

AN INVESTIGATION OF CAVITATING INDUCERS FOR TURBOPUMPS

1. INTRODUCTION

The desire to achieve satisfactory performance of centrifugal pumps at high suction specific speeds has led to investigations (1, 2, 3) recently of axial inducers as a possible solution. An inducer is an axial pump intended to be used in conjunction with a centrifugal pump. The usual configuration is shown in Fig. 1. It is expected that the inducer operate with cavitation, hence a diffusing section is usually allowed between inducer exit and pump inlet. The pressure rise produced by the inducer need only be sufficient to prevent cavitation in the main pump, so the inducer is usually lightly loaded.

The pumping of liquids at or near their vapor pressure can be difficult, and in conventional applications (condensate pumps, refineries, etc.), it is accomplished by using a larger than normal pump. However, in the present area of interest, i.e. turbopumps for large liquid rocket engines, pump size is of prime importance. It is desired to make the pump as light as possible (4). Since pump power is usually supplied by a gas turbine which in these applications is inherently a high rotative speed device, it would be advantageous to connect the impeller directly to the turbine and thereby eliminate heavy gearing. Also, in keeping propellant tank weight to a minimum, a low inlet pressure is unavoidable. All of these requirements call for a pump capable of operating at high suction specific speeds.

Inducers have been in use for some time in the liquid rocket engine field, but most of the work is classified in nature, thus limiting our knowledge of the present state of the art.

The purpose of this investigation is to determine design criteria for inducers capable of operating at high suction specific speeds.

2. DESCRIPTION OF INDUCERS

Two designs were tested. The analytical considerations for the first design are presented in Gas Turbine Laboratory Report No. 44 by A. H. Stenning, and will be briefly summarized here; blade shape at the tip was specified since this section is the most critical with respect to cavitation. Constant pressure was specified on the blade suction surface. Thus, at incipient cavitation the pressure along the suction surface at the blade tip equals the vapor pressure. For ease of manufacture, inducers were designed with radial blade elements (tangent of blade angle proportional to radius at any particular axial position). From radial equilibrium considerations, the axial velocity was determined as a function of blade angle (and therefore, radius). From these considerations, a blade shape equation is obtained. This blade shape differed only slightly from a true free vortex design (Fig. 1a). This inducer is referred to, throughout, as Stennings's design (Fig. 2).

Some initial difficulty was experienced in translating the theoretical tip coordinates into those useful to the machinist. A separate set of coordinates was needed for pressure side and suction side. In addition, since it was desired to have radial blade elements (at the blade

centerline), the milling cutter was offset from the centerline of the work by an amount that varied with the blade angle. A sample set of coordinates is shown in Table I. X is the axial coordinate, θ the angular rotation of the work, and Y, the cutter offset from the center line. Cuts were made in intervals of 2° and the blade surface finished by hand. The blades had a 2° taper (4° included angle) from tip to hub.

The second inducer tested had three blades with constant helical pitch and radial blade elements. Specifications for this are also shown in Fig. 2. This inducer is refered to as a flat plate inducer throughout the report.

3. EXPERIMENTAL APPARATUS

The test facility is a closed loop circuit designed specifically for testing axial inducers (Fig. 3). It has a capacity of 28 gallons, with a 1.8 in. diameter test section. The piping and valves are 3 in. diameter aluminum. The service and filter pumps (Fig. 3) are of the standard centrifugal type. The service pump has a capacity of 500 gpm. The filter is a standard commercial item capable of removing particles down to 25 microns diameter.

A simple, but effective, heat exchanger is used. It consists of a 12 ft. section of 4 in. pipe concentric with an equal length of 3 in. pipe. The coolant flows through the annulus in a counter flow direction. Thus, by controlling the coolant flow with a gate valve, the temperature of the test water can be controlled to within one degree Fahrenheit.

A layout of the test section and plenum chamber is shown in Fig. 4. A single 20 x 20 to the inch - mesh screen is used to trap any

large dirt particles. Some smaller mesh screens were tried but became partially blocked after a few hours running time. Distilled water was used throughout the testing to minimize the amount of dirt introduced.

A cylindrical sampling probe 1/2 in. in diameter with two holes of 0.040 in. diameter, arranged so that a continuous flow to and from the system is maintained, is mounted in the plenum. This sample is used for air content determination of the test water. A Van Slyke blood gas analyzer is used to process the sample (5).

A bundle of straightening tubes consisting of 3/8 in. thin walled aluminum tubing 5 in. long is used to give an axial inflow to the test section. These completely fill the 5 in. diameter passage.

The contraction from plenum to test section is designed according to Smith and Wang (6). The predicted variation in axial velocity at the contraction exit was less than 1/5 of one percent. A traverse was made with total pressure probe at the test section entrance and within the limits of the experiment no variation was discernible, i.e. less than 1% variation in velocity at a mean flow of 16.1 ft. per sec. The contraction is used to measure flow rate, and is calibrated against a 3 x 2.4 in. venturi meter. They agree within 0.005 cfs (4.5% max.) over the range tested.

The test section was bored from a piece of lucite tubing 6 1/2 in. long. The nominal diameter of the inducer tested is 1.800 in. The tip clearance allowed is such that the optimum value of the tip clearance parameter as defined by Rains (7) (tip clearance divided by maximum blade tip thickness) is obtained. This value is 0.098.

Somewhat larger clearances are used in practical rocket pumps (8), amounting sometimes to as much as 3% of the blade span. The necessary

clearance depends on the general rigidity of the pump sturcture, exterior loads, and the nature of the liquid being pumped. Rubbing must be avoided for some liquids.

Static pressure taps are located at the test section entrance just downstream of the contraction exit, and 0.150 in. downstream of the inducer exit. At each location, there are a set of taps at 90 degrees to each other. There is also a set of taps on the drive shaft housing in line with those on the test section casing. This allowed the static pressure to be measured both at the hub and tip at the inducer exit (station 3, Fig. 1). The set of taps are used to determine circumferential uniformity. The maximum circumferential non-uniformity observed did not amount to more than 2% of the pressure difference from hub to tip. Non-uniformity was present only at low flows and extreme cavitation conditions.

A three hole "cobra" probe is used for traversing the flow at inducer exit (Figs. 4, 5). It is constructed of three hypodermic tubes 0.018 in. diameter, so that the tip dimensions are 0.018 x 0.054. The time response of the probe to deviations from the flow direction is about three minutes to final equilibrium with a water-mercury manometer. The probe traversing mechanism permits travel in the radial direction with a precision of 0.001 in. The probe tip remains in the same plane as the static pressure taps when the probe is rotated. A yaw vernier allows the absolute flow exit angle to be measured within 0.2°. A cobra probe is sensitive to changes of this order, and the probe was calibrated for deviations from the flow direction. The method of using the probe was to align it approximately (within 1°) with the flow direction, read the pressure differential and correct the angle by means of a calibration curve. A zero angle is obtained by substituting a hub without blades in

place of the inducer and operating the service pump. This flow angle varies less than 1° from hub to tip. With the dummy hub in place, the friction and windage torque of the driving dynamometer, seals, bearings, and hub is obtained.

A simple scroll is used to diffuse the flow from the inducer. It is basically toroidal in shape with two exit pipes whose centerlines are tangent to the centerline of the toroid. It is machined in two halves from a solid block of aluminum. The mating faces are coated with an adhesive and the two halves bolted together.

The stainless-steel driveshaft is supported on one end by a sealed ball bearing and on the other by a water lubricated nylon bearing. There are two "Garlock Clozures" between the bearings to seal about the shaft.

A driving dynamometer designed by the Dynamic Analysis and Control Laboratory at M.I.T. drives the inducer. It has a three phase induction motor, the speed of which may be varied by varying the frequency of power input. A variable frequency motor-generator was used to supply power. The m - g set consists of a 400 cps self-excited aircraft generator and a variable speed drive.

At the start, the capabilities of the driving dynamometer were not known, since it was not designed specifically for this application. It soon became evident that power output was limited to about one horsepower at 10,000 rpm, and this with air-blast cooling of the motor. Time did not permit the redesigns that would have been necessary to fully rectify the situation. The motor-generator had to be modified slightly to obtain the low frequency power (200 cps) needed to run the dynamometer in the 10,000 rpm speed range. This modification cut out the generator

speed control. Thus no motor speed control is possible in the speed range tested. Motor speed was determined by motor characteristics and the applied load.

The drive motor is swung on an air bearing. With a linearsyn and leaf spring arrangement (Fig. 6) the torque is read on an electronic volt meter sensitive to 0.003 ft-lb.

A speed counter device consisting of a permanent magnet within a coil and an arm that rotates with the driveshaft (Fig. 6) is used to determine the rpm of the inducer. When the arm cuts through the gap it produces a signal in the coil. This signal is filtered and then counted with a Hewlitt-Packard electronic counter. This checked with the speed when measured by a Strobotac to within 1%.

Originally it was intended to test a 2 in. diameter inducer, but in order to reduce the power requirement it was found necessary to reduce the diameter.

4. TEST PROCEDURE

Pump Performance

Before each pump performance (non-cavitating) test, the water was circulated through the filter for two hours to remove any foreign particles. This was intended as an aid in preventing the probe from becoming clogged. During eight months of testing the probe became stopped up once. Erratic readings made this immediately obvious.

After filtering, the inducer was started and the desired flow coefficient established by manipulating the throttle and bypass valves.

The service pump was used at larger flows to overcome head loss in the return pipes.

Cooling air for the drive motor and air bearing was turned on. Cooling water for the heat exchanger was turned on and the flow adjusted until the water temperature stabilized at about 70°F. The electronic equipment was allowed to warm up. Total warm up time was one-half hour.

The probe was set 0.050 in. from the hub and moved in steps of 0.050 in. toward the tip. Stagnation pressure was recorded to the nearest 0.01 in. and the flow direction to the nearest 0.2°. Also recorded were the static pressure rise across the inducer at the tip and the difference in static pressure from hub to tip. The static depression across the contraction and the static pressure at the entrance to the contraction were recorded.

From this, the stagnation pressure at each probe position was plotted. Then, assuming a linear variation of static pressure from hub to tip, the axial velocity distribution at the inducer exit was calculated. This approximation was improved in a few cases by considering radial pressure variation satisfying simple radial equilibrium. The axial velocity distribution found in this manner was nearly the same as that found by the assumption of linear pressure variation, therefore, the calculation was not carried out for all cases. For tests in which back flow was observed, static pressure was assumed constant in the backflow region. This is equivalent to assuming no flow in this region.

The total mass flow roughly calculated in this manner differed from that calculated from the static depression across the nozzle by a maximum of 15%. This computed axial velocity distribution was used to mass-average the head rise.

Torque was indicated on a vacuum tube voltmeter and the torque

sensing device calibrated after each run by means of a pan balance and weights hung on an arm attached to the motor housing (Fig. 6).

Cavitation Performance

In starting up for a cavitating performance run, the procedure is somewhat more complicated. The test water must be deaerated as thoroughly as possible to minimize the effects of cavitation inception from gas nuclei, or perhaps it would be better to say to standardize the results (9). Deaeration was accomplished by lowering the system pressure to the minimum value attainable with a vacuum pump and circulating with the filter pump for one hour. The vacuum was then released and the air which had collected in the high spots of the system bled off. Air content was measured with a Van Slyke apparatus (5). This process was repeated until the total air content as indicated by the apparatus attained some arbitrary low value. Since the apparatus indicates the total air content (both dissolved and undissolved), the arbitrary value for maximum air content was set at 5 ppm (by weight). This represents 23% of the saturated air content of water at 20° C. and atmospheric pressure (10).

It is recognized (9, 11) that the onset of cavitation in liquids is caused by the presence of gas nuclei and that for liquids containing relatively large nuclei, cavitation will occur at pressures higher than the vapor pressure. Of the two general types of cavitation, vaporous and gaseous, vaporous is the more important because of its sudden, explosive rate of growth and collapse. Also, vaporous cavitation can only occur at pressures below the vapor pressure; and for nuclei with radii smaller than 10^{-3} cm. the inception pressure is negative. Thus a variation in the size and number of gas nuclei can introduce scale effects.

That is, for flow about large bodies with small pressure gradients at low mean flow velocities, nuclei will have more time to grow. Whereas, for flow about small bodies with steep pressure gradients at relatively high mean flow velocities, nuclei will not cause cavitation if they are smaller than a certain (calculable) size.

The system pressure was reduced in steps of approximately two inches of mercury. The same readings were taken as in the non-cavitating performance runs except that the probe remained fixed at 95% of the tip radius. Barometric pressure was recorded.

The system pressure was reduced until pressure readings became unreliable due either to unsteadiness or to the formation of bubbles in the manometer lines. At this point control of the flow rate was also difficult.

Cavitation runs at the higher flow rates were not possible because of extensive cavitation in the entire system piping. If, during a given reduction in pressure, the rpm of the inducer changed slightly because of a change in the blade loading, the flow rate was adjusted until the desired flow coefficient was reestablished. Thus during a cavitating performance run, the inducer rpm was not constant, but varied usually by less than $\pm$ 1%.

A description of the cavity formation was recorded and this information used to determine when pictures of the cavitation should be taken. A Fastax camera was used with 3500 watts of incandescent lighting. Pictures were taken at the rate of 10,000 per second for Stenning's design and at 11,000 per second for the flat plate inducer. For the runs during which pictures were taken, the data recorded were: inducer speed,

flow rate, static pressure at contraction entrance, and barometric pressure.

5. PRESENTATION OF DATA

The non-cavitating pump performance data is presented in a conventional manner of head, power, and efficiency, all versus flow rate, except that these have all been non-dimensionalized, i.e.

Head coefficient

$$\psi = \frac{\Delta H}{U_t^2/g}$$

Flow coefficient

$$\varphi = \frac{C_x}{U_t}$$

Torque coefficient

$$\tau = \frac{T}{\rho A U_t^2/g}$$

and efficiency

$$\eta = \frac{\varphi \psi}{\tau}$$

Also plotted are aboslute exit angle, relative exit angle, axial velocity distribution, and tangential velocity distribution, all versus a dimensionless radius, R/R_{tip}.

In presenting the cavitating performance data, the head, power, and efficiency are plotted against Prandtl's cavitation parameter, K,

$$K = \frac{P - Pv}{W^2/2g}$$

Where Pv is the vapor pressure, W the relative fluid velocity at station 1 (Fig. 1), and P is the static pressure at 1. The pressure at station 1 is calculated from the static pressure at the contraction entrance, flow rate, and test section geometry. A static pressure tap was placed at 1, but it was discovered that significant errors were present when compared with the static pressure calculated. Also, it was difficult to keep bubbles from forming in this manometer line at low system pressures.

The point of breakdown inception (where the head has fallen off to 90% of its non-cavitating value) is presented as is the suction specific speed. This suction specific speed is calculated at the nearest data point to the point of breakdown inception.

6. DISCUSSION OF RESULTS

6.1 Non-Cavitating Performance

The non-cavitating pump performance data for both inducers is presented in Fig. 7. Each inducer was tested over a range of flows on both sides of its point of best efficiency.

A maximum efficiency for Stenning's design of 86% was observed at a flow coefficient of 0.17. The design flow coefficient was 0.227 at which the efficiency was 80%. The maximum efficiency observed for the flat plate inducer was 72% and this at a flow coefficient of 0.152. Perhaps a more useful comparison would have resulted if the two inducers had been designed to give equal head rise at the same flow coefficient. This will be borne out later in the discussion on cavitating performance.

Absolute exit flow angles are presented in Figures 8 and 9.

Back flow regions at the hub are evident at small flows. The increased turning at hub and tip is due in part to boundary layer buildup on the hub and casing.

Axial velocity distribution is shown in Figs. 10 and 11. For Stenning's design the axial velocity distribution at the point of best efficiency was observed to approximate closest the design distribution determined from radial equilibrium considerations. However, Fig. 12 shows that at the point of best efficiency the observed tangential velocity distribution is radically different than the design distribution. A comparison between test results and design is of questionable validity at those extreme off-design conditions.

Figs. 16 and 16a show the relative flow exit angles. The flow deviation angle was predicted from Carter's rule (12). Again a comparison is valid only at the design point. The flow pattern is obviously more complex than was predicted on a two-dimensional basis. It is interesting to note that even though the inducer (Stenning's) had a solidity at the tip of 2.02, the relative flow angle exhibits a large deviation from the blade angle. A better method of predicting deviation angle would be very desirable.

6.2 Cavitating Performance

The cavitating performance of head, torque, and efficiency are presented in Figs. 17 through 20. For some runs there was a slight increase in one or more of these quantities just prior to the point where the head began to deteriorate because of severe caviation. The efficiency may have increased slightly because of the decrease in friction losses on the blades. For the flat plate inducer it was observed that the head

did not begin to fall off until the cavity formation (which started at the leading edge of the blade) had extended to the trailing edge, and then, quite suddenly. Whereas for Stenning's design the head fell off gradually as the cavity formation grew toward the trailing edge.

The variation of cavitation number at the point where the head has fallen off to 90% of its value at non-cavitating conditions, with flow coefficient is presented in Fig. 21 for both designs. This can be misleading however, because the rate of deterioration is not the same for both inducers, nor for all runs on each design. For Stenning's design at flows near the design point the deterioration is gradual, while for low flows (solid-body rotation, Fig. 12) the head decay is more rapid. The flat plate inducer, which always operates at positive angles of attack showed this abrupt breakoff at all flows. It is usually thought that if a cavitating machine is properly designed, best performance will result at zero angle of incidence, thus it was expected that Stenning's design would be best at the design point. It was anticipated that the liquid entering the inducer be at or near its vapor pressure, at which condition it can suffer very little acceleration without cavitating. Consequently the rate of turning was quite small at the beginning of the blade and increased rapidly near the trailing edge. This caused cavitation towards the trailing edge at design flow and resulted in breakdown sooner than expected. A solution to this would be to lengthen the inducer and introduce the turning more gradually.

It was intended that all three of the inducer blades have the same dimensions. However due to a machining error one blade on the inducer of Stenning's design was slightly thinner than the other two, i.e. 0.030 in. at the tip and 0.060 in. at the root. This was observed to

have a deterring effect on the formation of cavitation on that blade (Figs. 25b, 26a). It was decided then to make the blades on the flat plate inducer somewhat thinner than those on the first inducer tested. The blades on the flat plate inducer were all the same dimension-wise as accurately as could be measured, but again cavitation seemed to favor two of the three blades, (Figs. 28c, 29b, 30a, 30c). Upon observing the leading edge of the blade that showed this reluctance to cavitate it was noticed that the tip had been rounded off slightly (during the finishing process after machining). Thus it would seem desirable to avoid a "square" leading edge tip.

Let us look at the dependence of suction specific speed on inducer characteristics at the blade entrance.

$$SSS = \frac{N\sqrt{Q}}{H_s^{3/4}}$$

or

$$\frac{N\sqrt{Q}}{H_s^{3/4}} = \frac{N\sqrt{C_{x_1}\frac{\pi}{4}(D_t^2 - D_H^2)}}{H_s^{3/4}}$$

assuming no prerotation. H_s can be expressed in terms of the inlet blade angle and a pressure coefficient, C_p,

$$C_p = \frac{P - P_{min}}{W^2/2g}$$

That is

$$\frac{H_s}{C_{x_1}^2/2g} = 1 + C_p + \frac{C_p}{\varphi^2}$$

and thus

$$\frac{N\sqrt{Q}}{H_s^{3/4}} = \frac{N\sqrt{C_{x_1}\frac{\pi}{4}D_t^2\left(1-\frac{D_H^2}{D_t^2}\right)}}{\left[C_{x_1}^2/2g\left(1+C_p+C_p/\varphi^2\right)\right]^{3/4}}$$

$$= \frac{D_t N\sqrt{\frac{\pi}{4}(1-r^2)}}{C_{x_1}\left[1/2g\left(1+C_p+C_p/\varphi^2\right)\right]^{3/4}}$$

where r is the hub-tip ratio and $D_tN = \frac{U_t 60}{\pi}$.

Therefore:

$$\frac{N\sqrt{Q}}{H_s^{3/4}} = \frac{60/\pi\sqrt{\pi/4\,(1-r^2)}}{\varphi\left[1/2g\left(1+C_p+C_p/\varphi^2\right)\right]^{3/4}}$$

From this suction specific speed has been plotted against flow coefficient for some values of C_p (Fig. 22). There is an especially strong dependence of suction specific speed on inlet angle ($\tan\beta = \frac{1}{\varphi}$) at low values of C_p. For incipient cavitation P_{min} is equal to P_v and therefore

$$C_P = K.$$

From Fig. 22 it appears easier to make a high suction specific speed machine when ϕ is small. Therefore comparison of inducers should be at equal values of ϕ and head rise. In order to fulfill this condition another inducer, after Stenning, with a smaller design flow coefficient should be tested.

The maximum values for suction specific speed obtained at breakdown inception were 27,600 for the flat plate design and 20,300

for the design after Stenning (Fig. 23).

CONCLUSIONS

A simple two-dimensional analysis is not sufficient to predict the performance of this type machine.

Although the performance was not as predicted, good efficiencies were obtained for both inducers tested. And lest we despair slightly about the value of analytical designs for axial flow pumps, the observed maximum efficiency for the analytical design was 14% higher than that for the simple flat plate design.

Inducers that operate at positive angles of incidence show an abrupt deterioration of head once the cavity formation has reached the inducer exit. When operating at or near zero angle of incidence the head is more gradual.

Operation at high suction specific speeds depends to a great extent on the success of the designer in producing inducer blading which will operate at low minimum pressure coefficients.

BIBLIOGRAPHY

1. Wislicenus, G. F., "Critical Considerations on Cavitation Limits of Centrifugal and Axial Flow Pumps", Trans. A.S.M.E., Nov. 1956.

2. Ross, C. C. and Banerian, G., "Some Aspects of High-Suction Specific-Speed Pump Inducers", Trans. A.S.M.E., Nov. 1956.

3. Nawoj, Henry John, "Cavitation Studies in Axial Inducers", A.E. Thesis, C.I.T., 1956.

4. Sutton, G. P., "Rocket Propulsion Elements", John Wiley and Sons, N.Y., 1956.

5. Peters, J. P. and Van Slyke, D. D., "Quantitative Clinical Chemistry", Vol. II, Williams and Wilkins Co., 1932.

6. Smith, R. H. and Wang, Chi-Teh, "Contracting Cones giving Uniform Throat Speeds", Journal of the Aeronautical Sciences, Vol. II, No.4, Oct. 1944.

7. Rains, Dean A., "Incipient Cavitation in Axial Flow Pumps, Part I; Tip Clearance Flows and Incipient Cavitation", Report E56.1, March 1954, Hydrodynamics Lab C.I.T.

8. Brennan, W. J., (Manager-Components Group, Rocketdyne), Personal communication.

9. Strasberg, M., "The Influence of Air-Filled Nuclei on Cavitation Inception", Report 1078, David Taylor Model Basin, May 1957.

10. Handbook of Physics and Chemistry, 34th Edition.

11. Daily, J. W. and Johnson, V. E. Jr., "Turbulence and Boundary Layer Effects on the Inception of Cavitation from Gas Nuclei", Technical Report No. 21, Hydrodynamics Laboratory, M.I.T., July 1955.

12. Howell, A. R., "Fluid Dynamics of Axial Compressors", The Institution of Mechanical Engineers, Proceedings 1945, Vol. 153.

13. Stenning, A. H., "The Design of Axial Inducers for Turbopumps", Gas Turbine Laboratory Report No. 44, Jan. 1958, M.I.T.

TABLE I - BLADE CUTTER COORDINATES

θ	X Pressure	Y Offset	X Suction
0	0.253	.027	0
10	.287	.027	0.033
20	.323	.027	.066
30	.359	.027	.100
40	.396	.027	.137
50	.434	.027	.176
60	.472	.027	.215
70	.510	.027	.254
80	.548	.027	.293
90	.586	.028	.333
100	.625	.028	.373
110	.664	.028	.414
120	.704	.029	.455
130	.744	.029	.496
140	.785	.030	.537
150	.827	.030	.578
160	.869	.031	.620
170	.912	.032	.662
180	.956	.033	.706
190	1.003	.034	.753
200	1.052	.036	.803
210	1.106	.039	.857
220	1.160	.042	.915
230	1.229	.046	.989

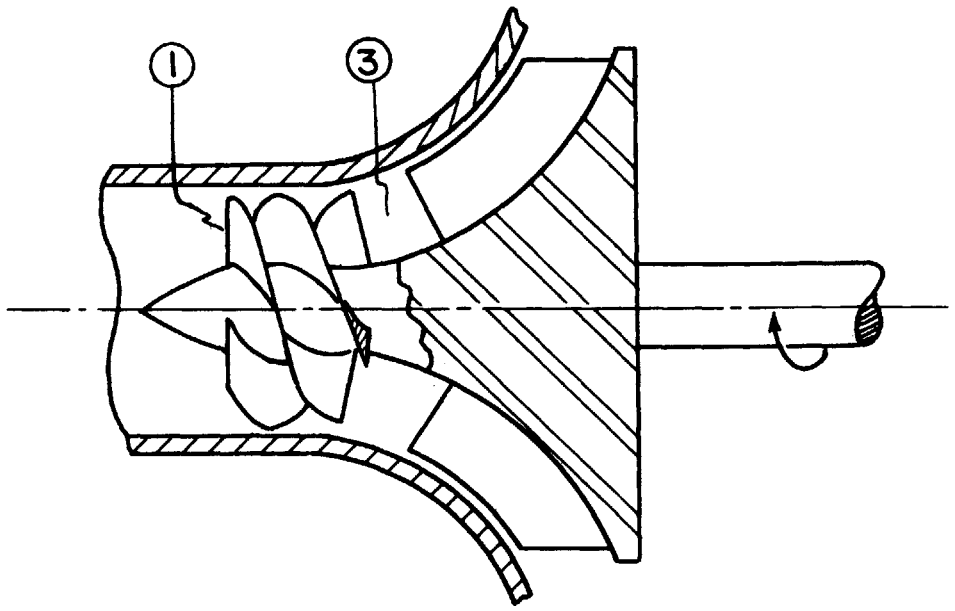

FIG. 1- PUMP WITH INDUCER

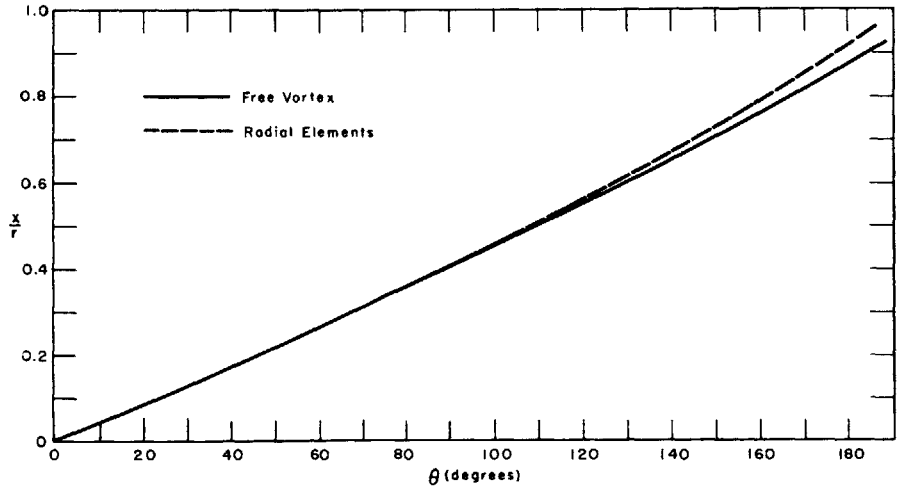

FIG. 1A- INDUCER TIP COORDINATES

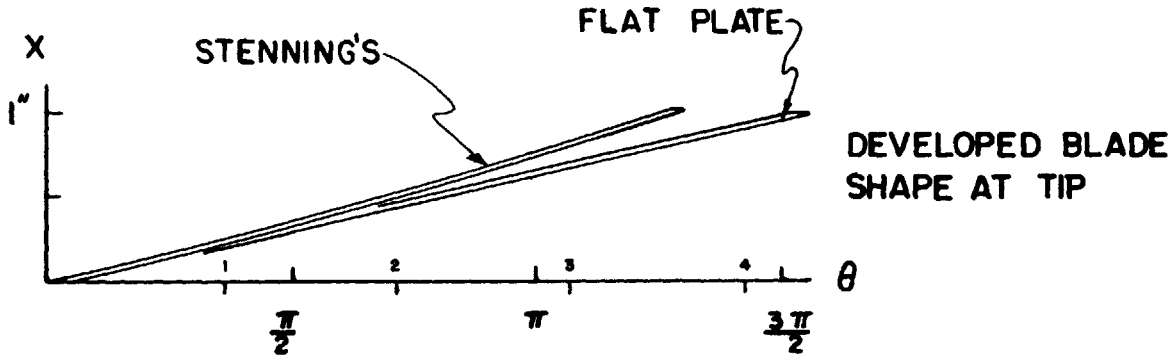

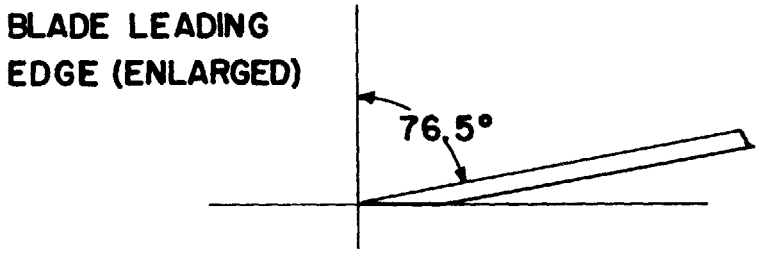

BLADE ANGLES	STENNING'S	FLAT PLATE
LEADING EDGE TIP	76.5°	76.5°
TRAILING EDGE TIP	65.5°	76.5°
DIMENSIONS		
THICKNESS AT TIP	.035	.030
THICKNESS AT HUB	.070	.060
DIAMETER	1.800	1.800
LENGTH	.978	.978
HUB - TIP RATIO	.444	.444
NUMBER OF BLADES	3	3

FIG. 2 - INDUCER SPECIFICATIONS

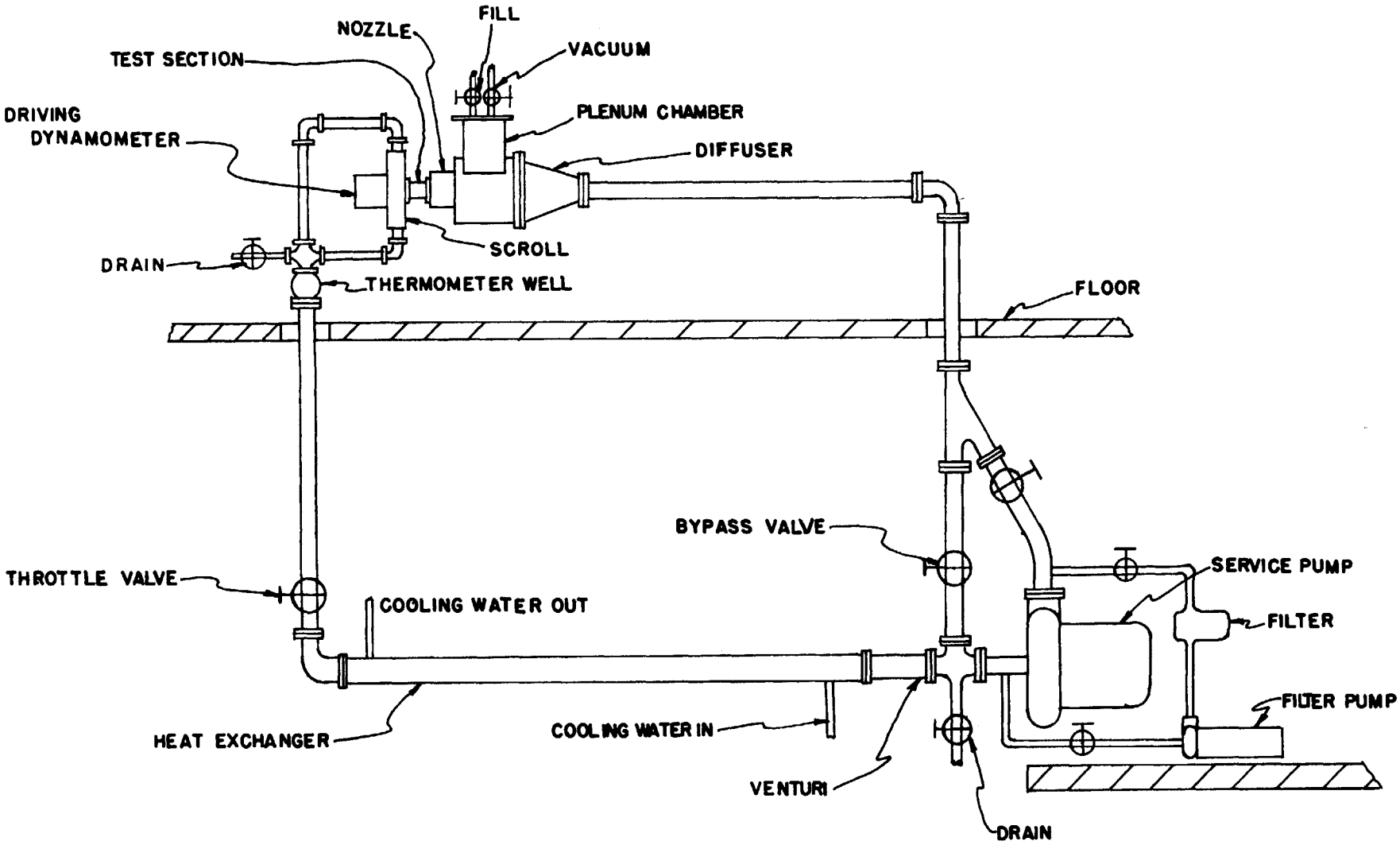

FIG. 3 - AXIAL INDUCER TEST FACILITY

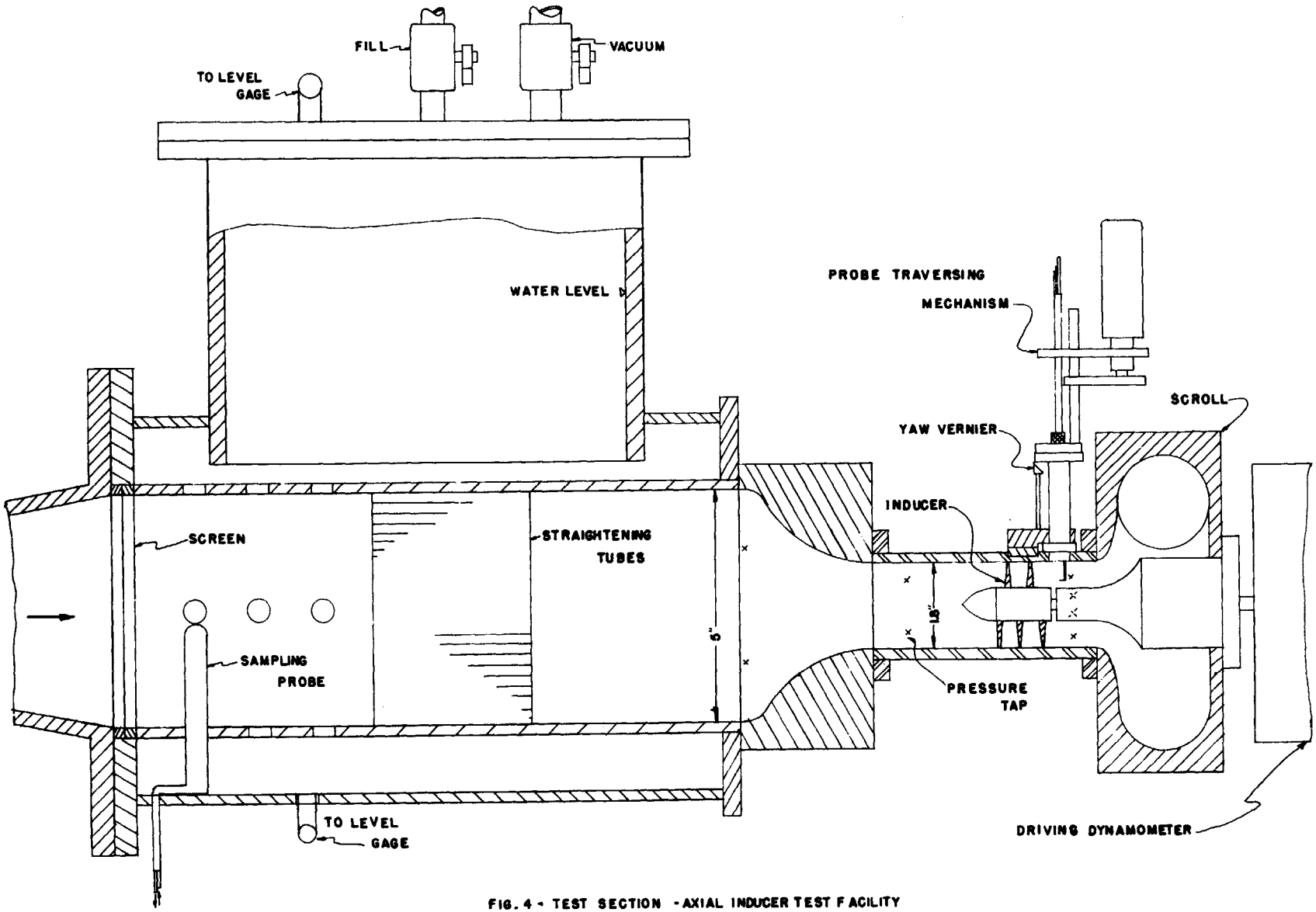

FIG. 4 - TEST SECTION - AXIAL INDUCER TEST FACILITY

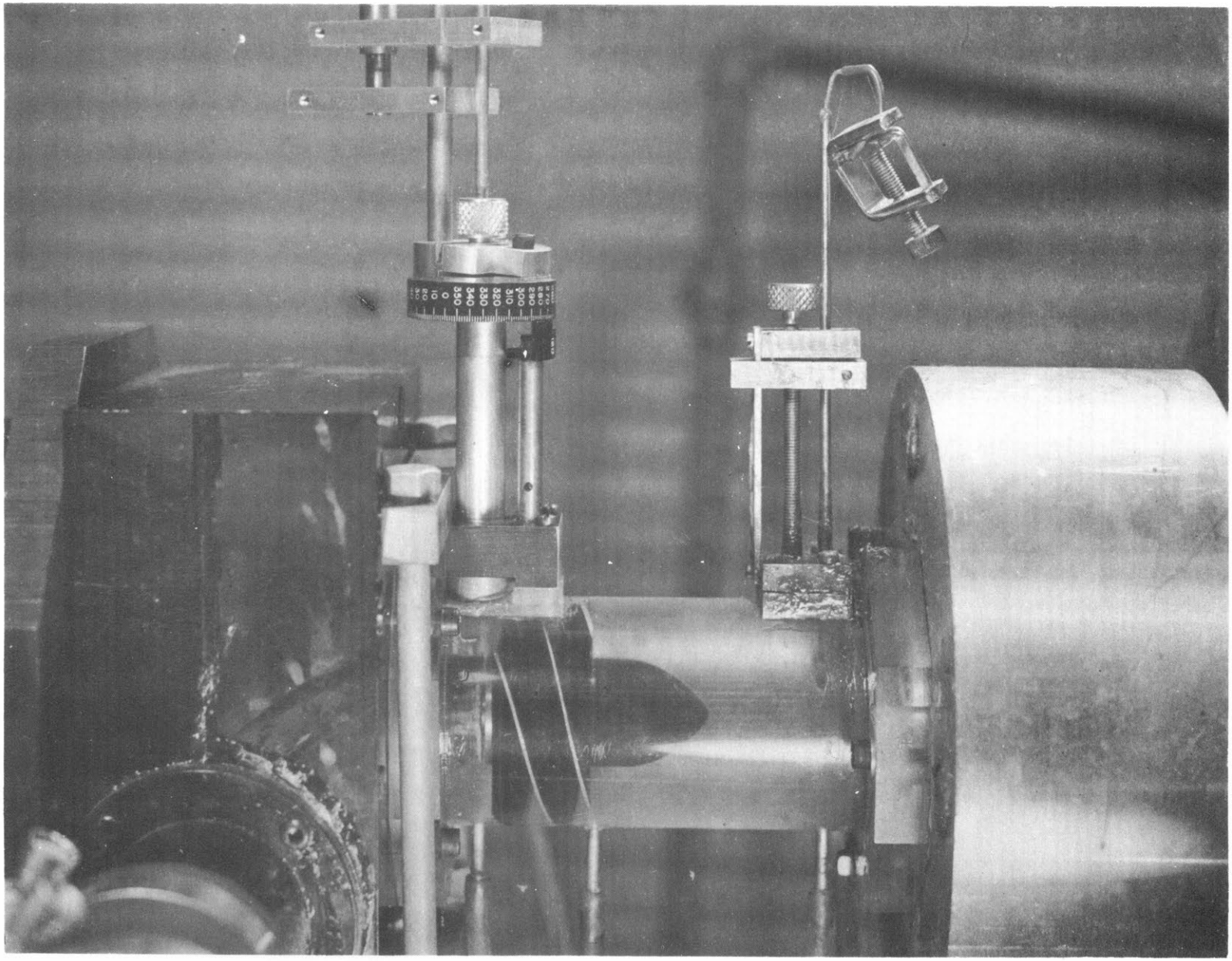

FIG. 4A-TEST SECTION

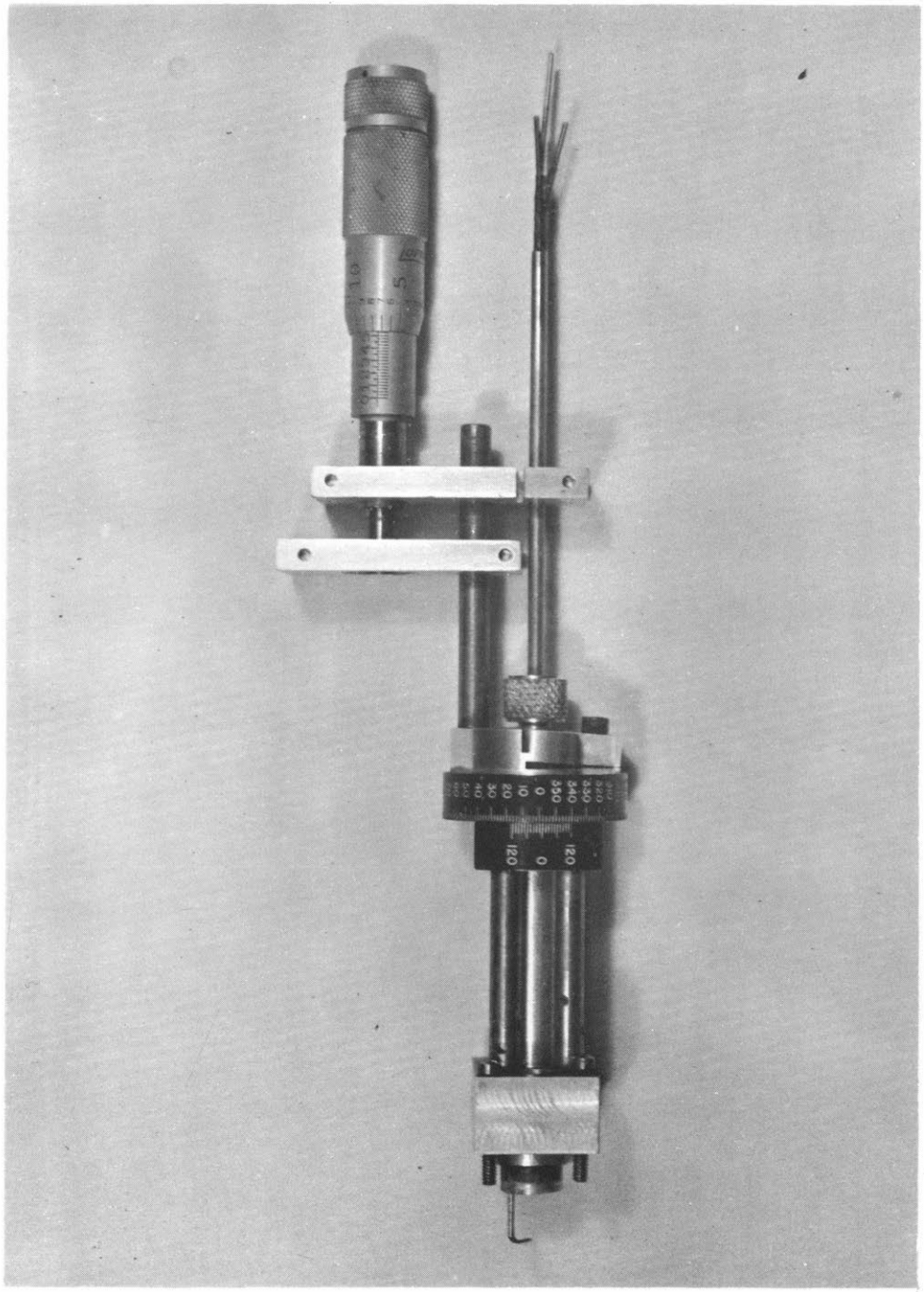

FIG. 5 - PROBE & TRAVERSING MECHANISM

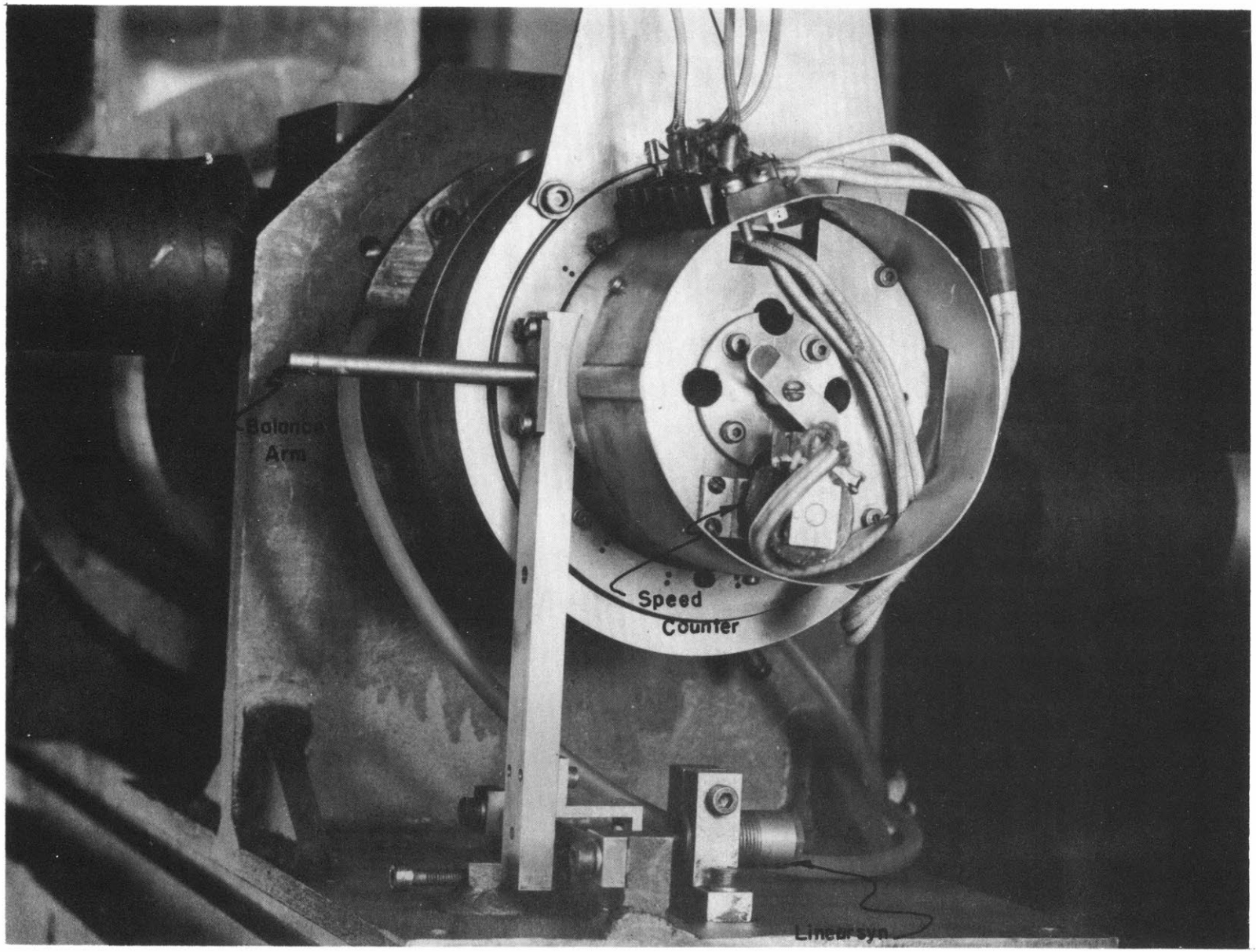

FIG. 6- DRIVING DYNAMOMETER

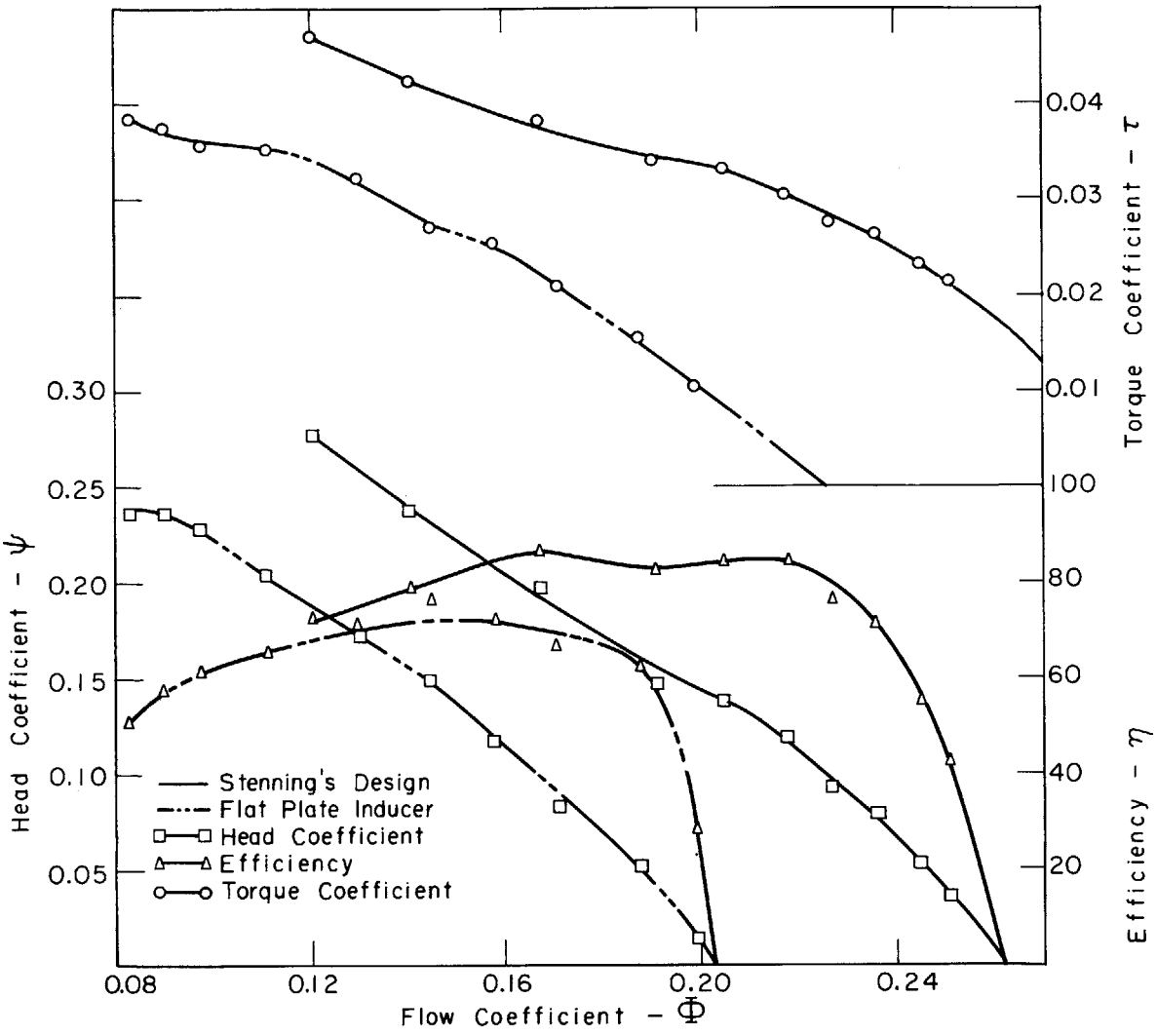

FIG. 7 NON-CAVITATING PUMP PERFORMANCE

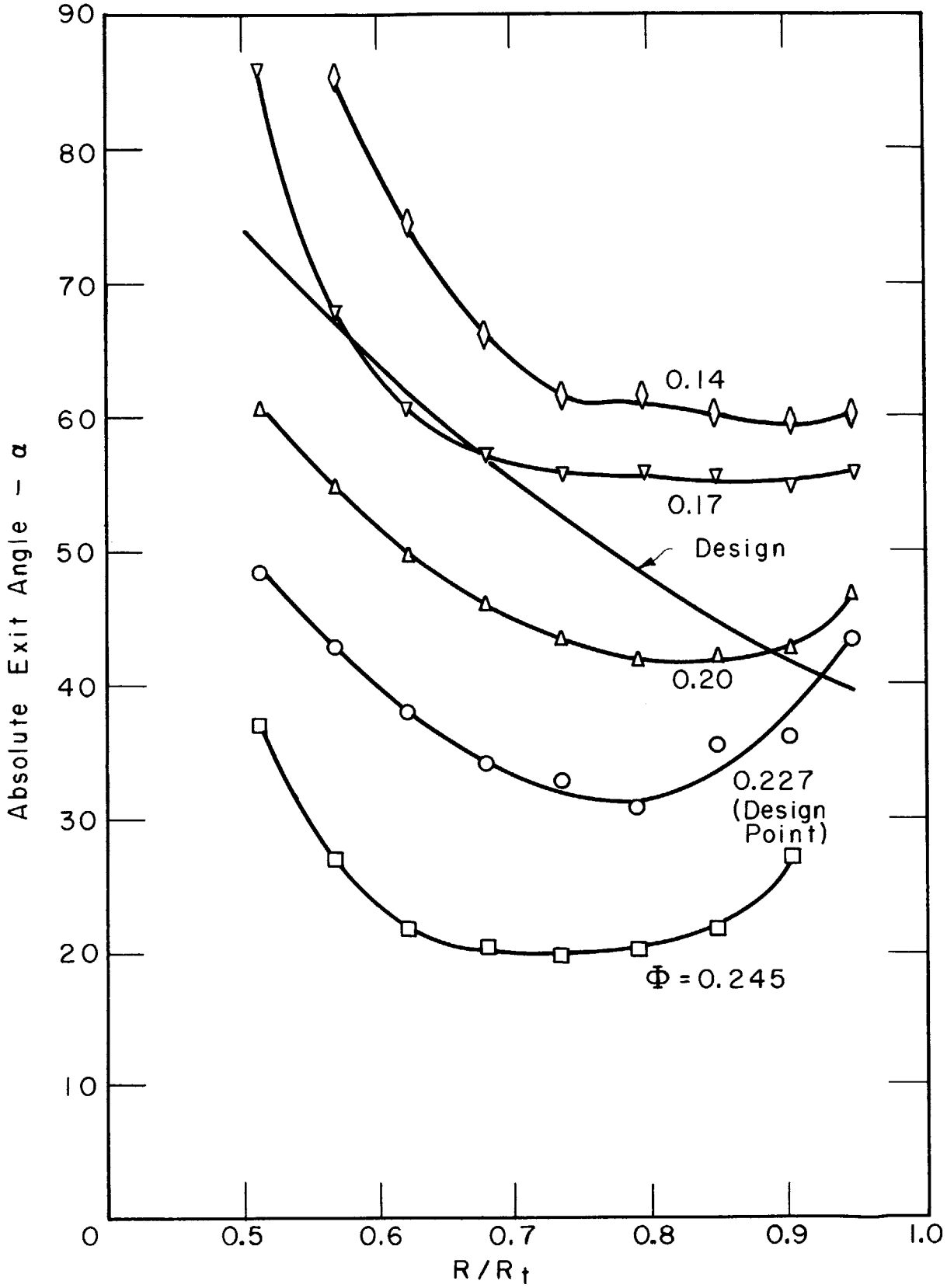

FIG. 8 ABSOLUTE EXIT ANGLE - STENNING'S DESIGN

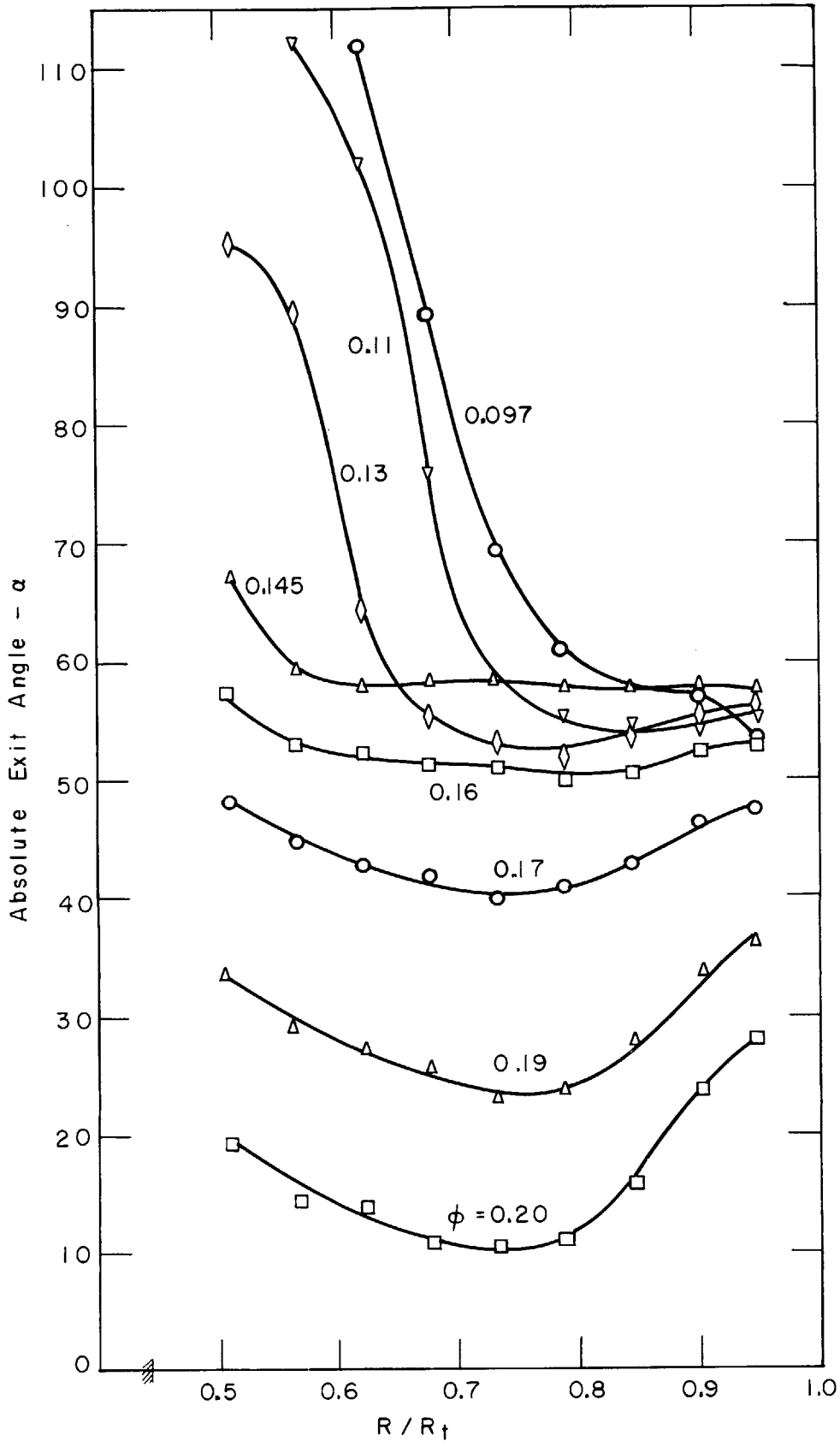

FIG. 9 ABSOLUTE EXIT ANGLE - FLAT PLATE INDUCER

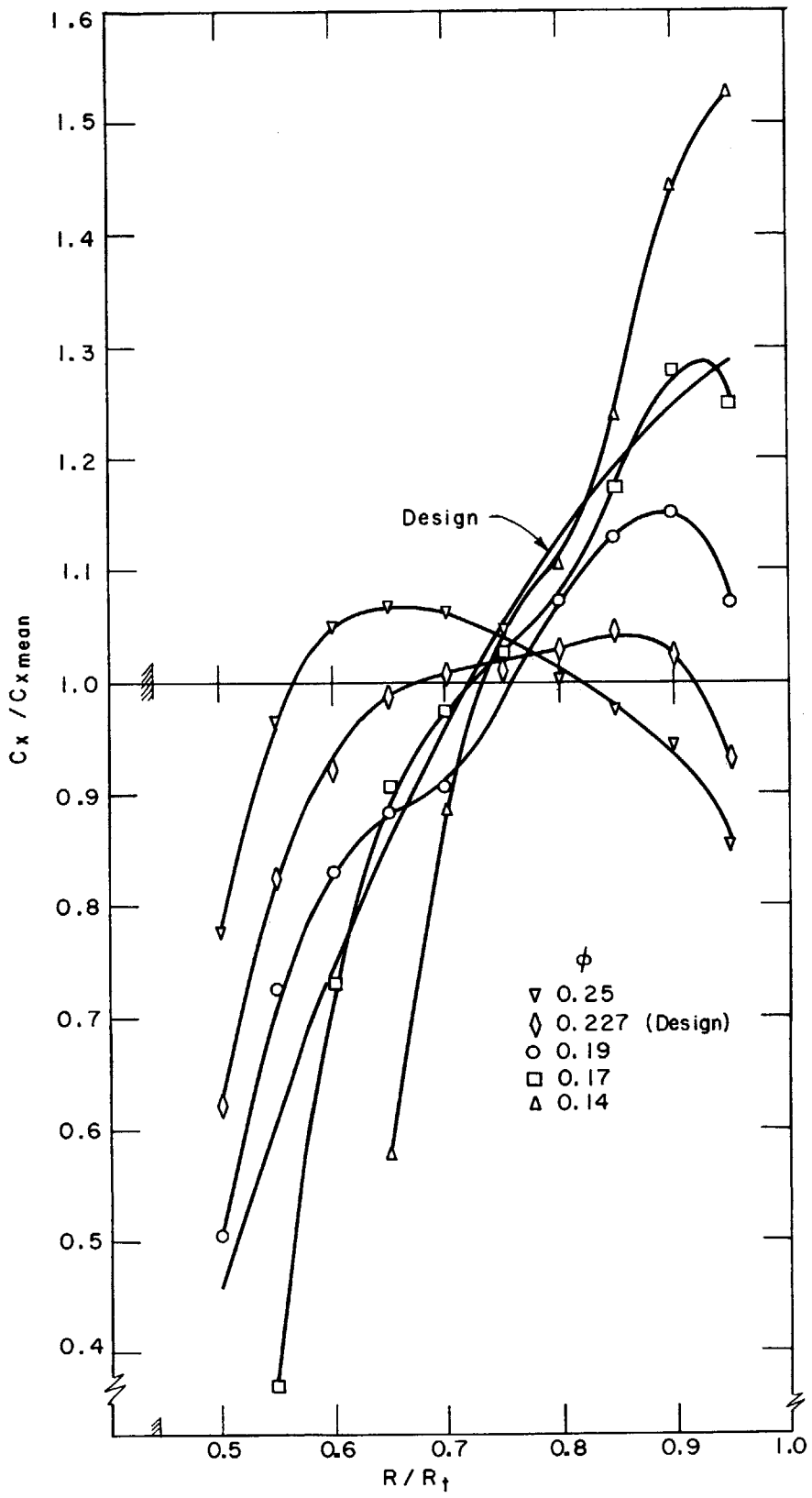

FIG. 10 AXIAL VELOCITY DISTRIBUTION - STENNING'S DESIGN

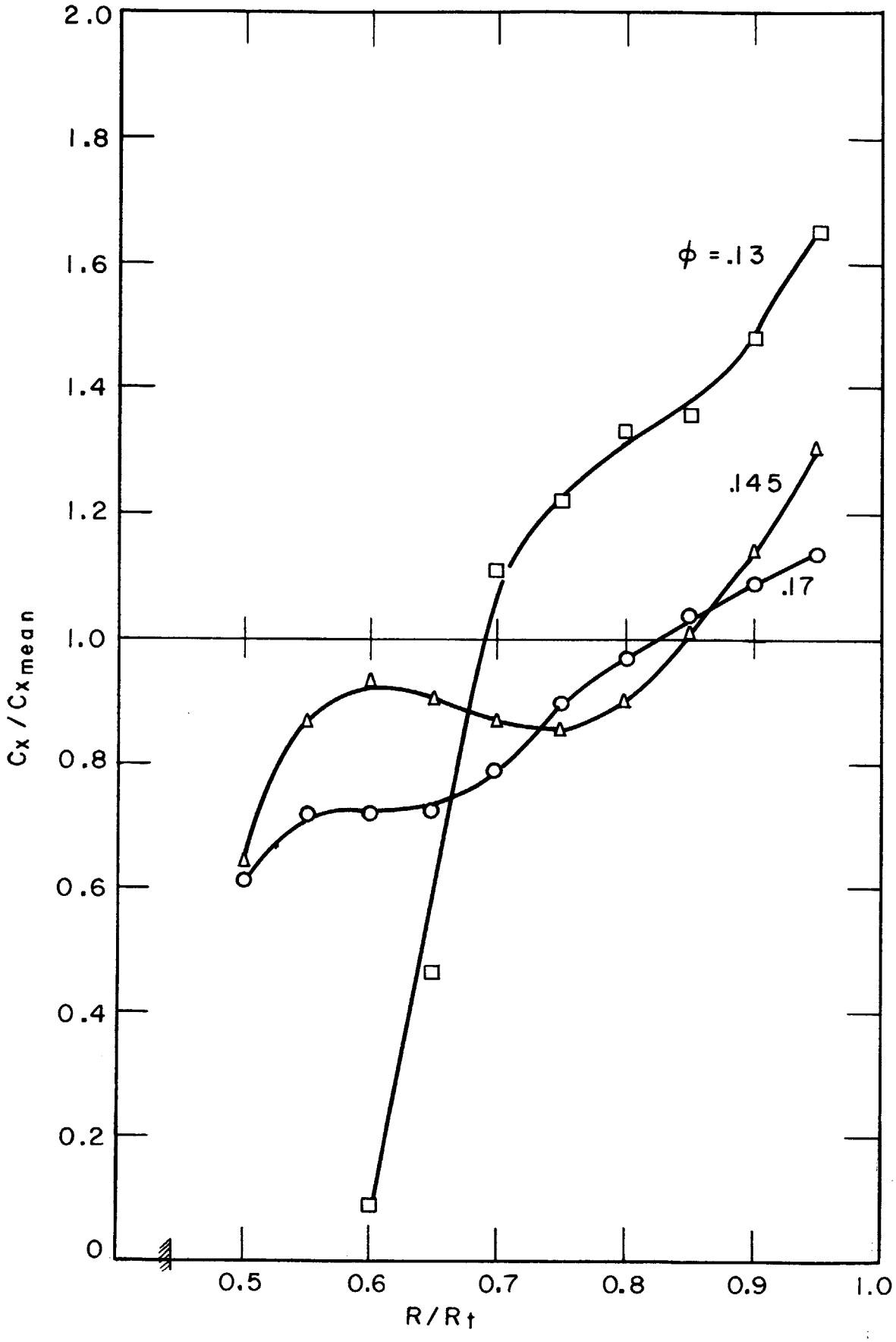

FIG. 11 AXIAL VELOCITY DISTRIBUTION - FLAT PLATE INDUCER

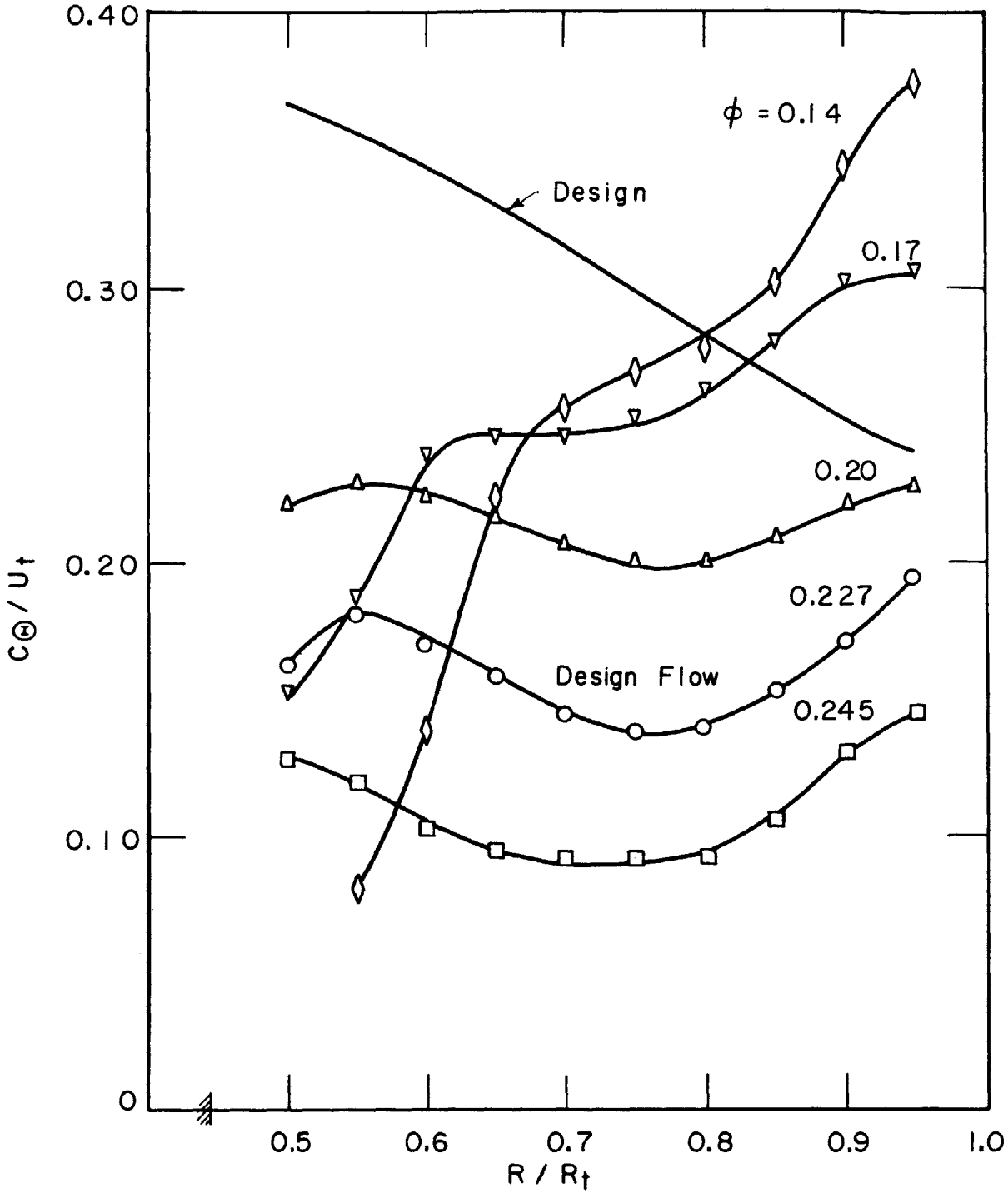

FIG. 12 TANGENTIAL VELOCITY DISTRIBUTION STENNING'S DESIGN

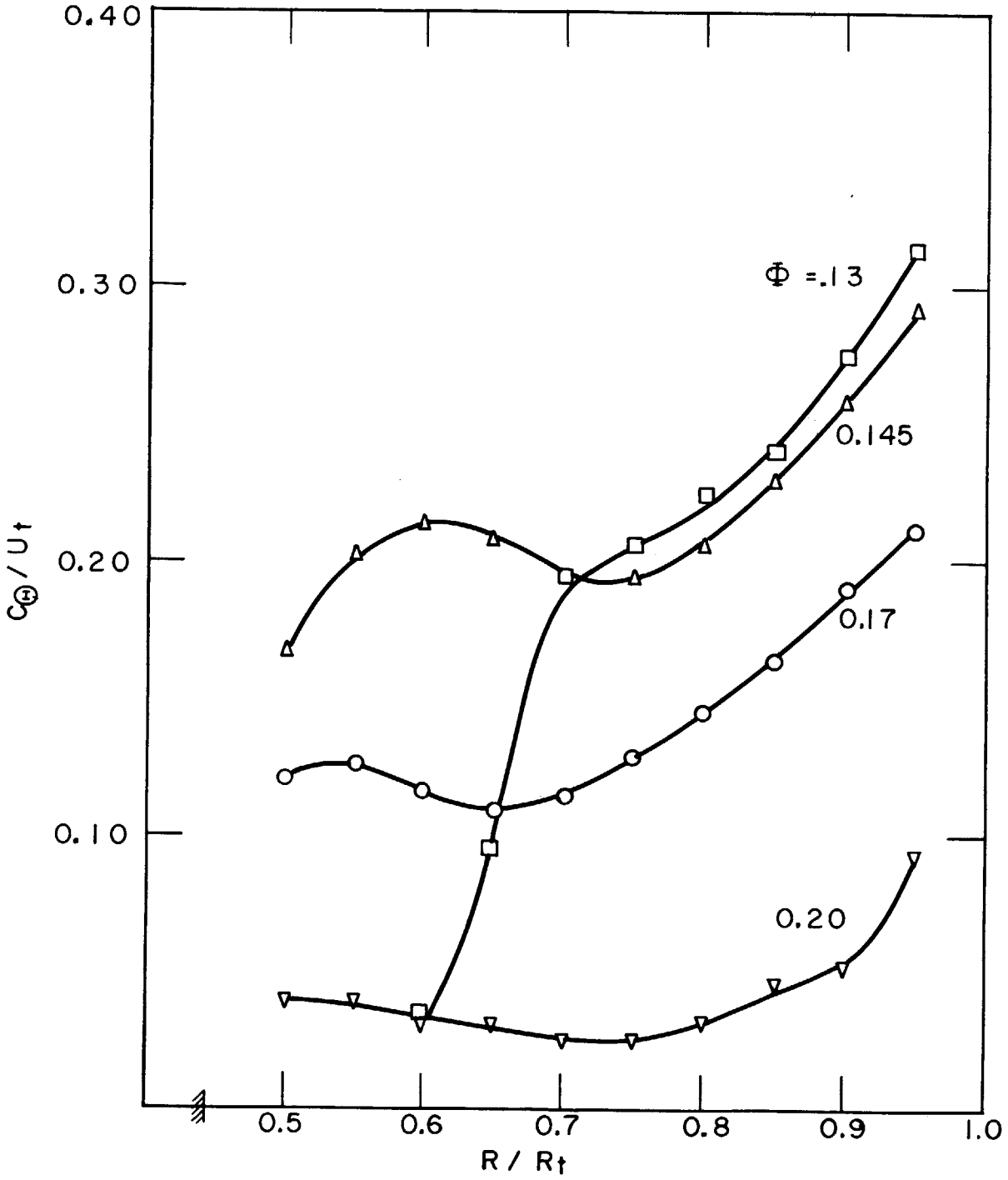

FIG. 13 TANGENTIAL VELOCITY DISTRIBUTION
FLAT PLATE INDUCER

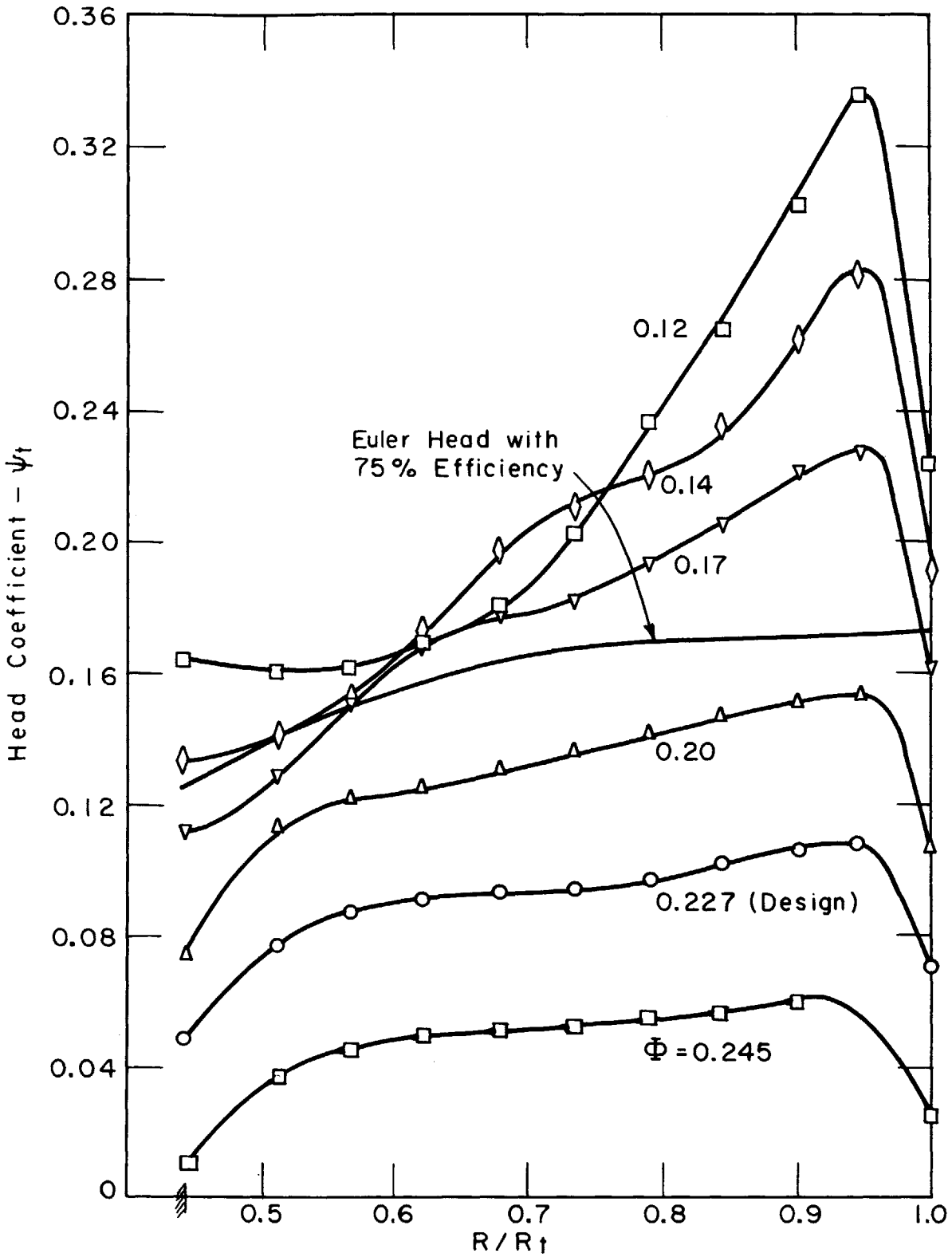

FIG. 14 HEAD COEFFICIENT – STENNING'S DESIGN

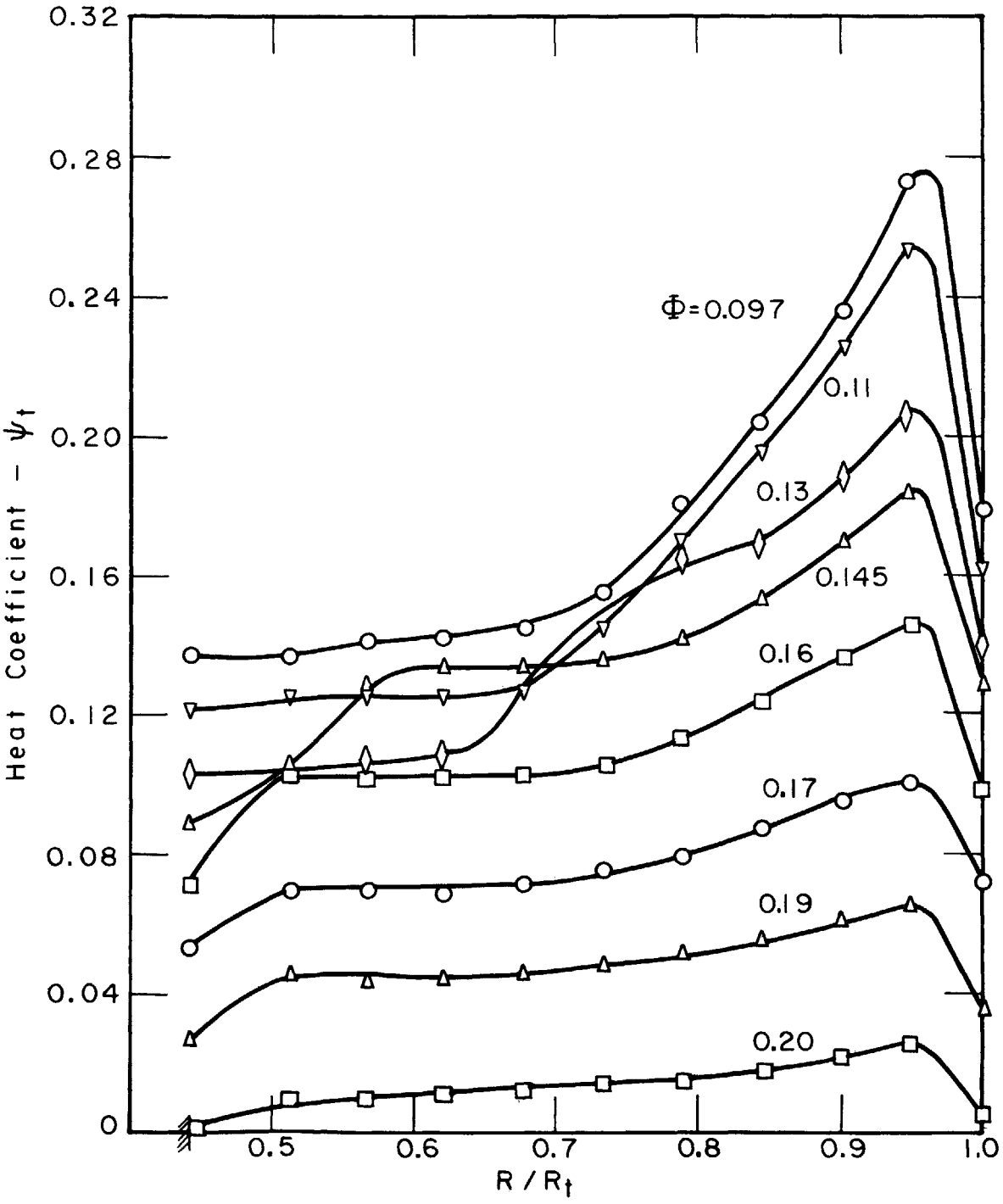

FIG. 15 HEAT COEFFICIENT - FLAT PLATE INDUCER

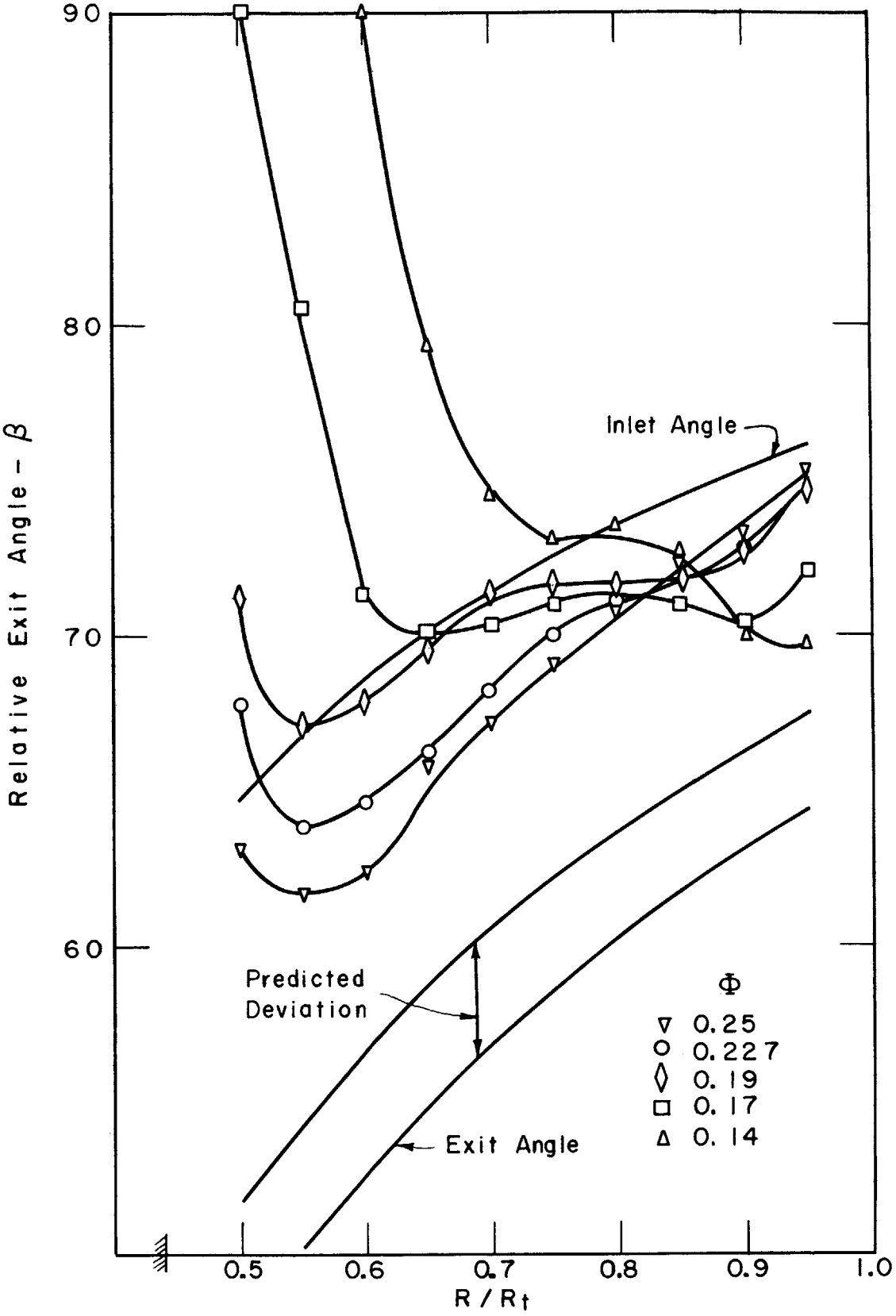

FIG. 16 RELATIVE EXIT ANGLE - STENNING'S DESIGN

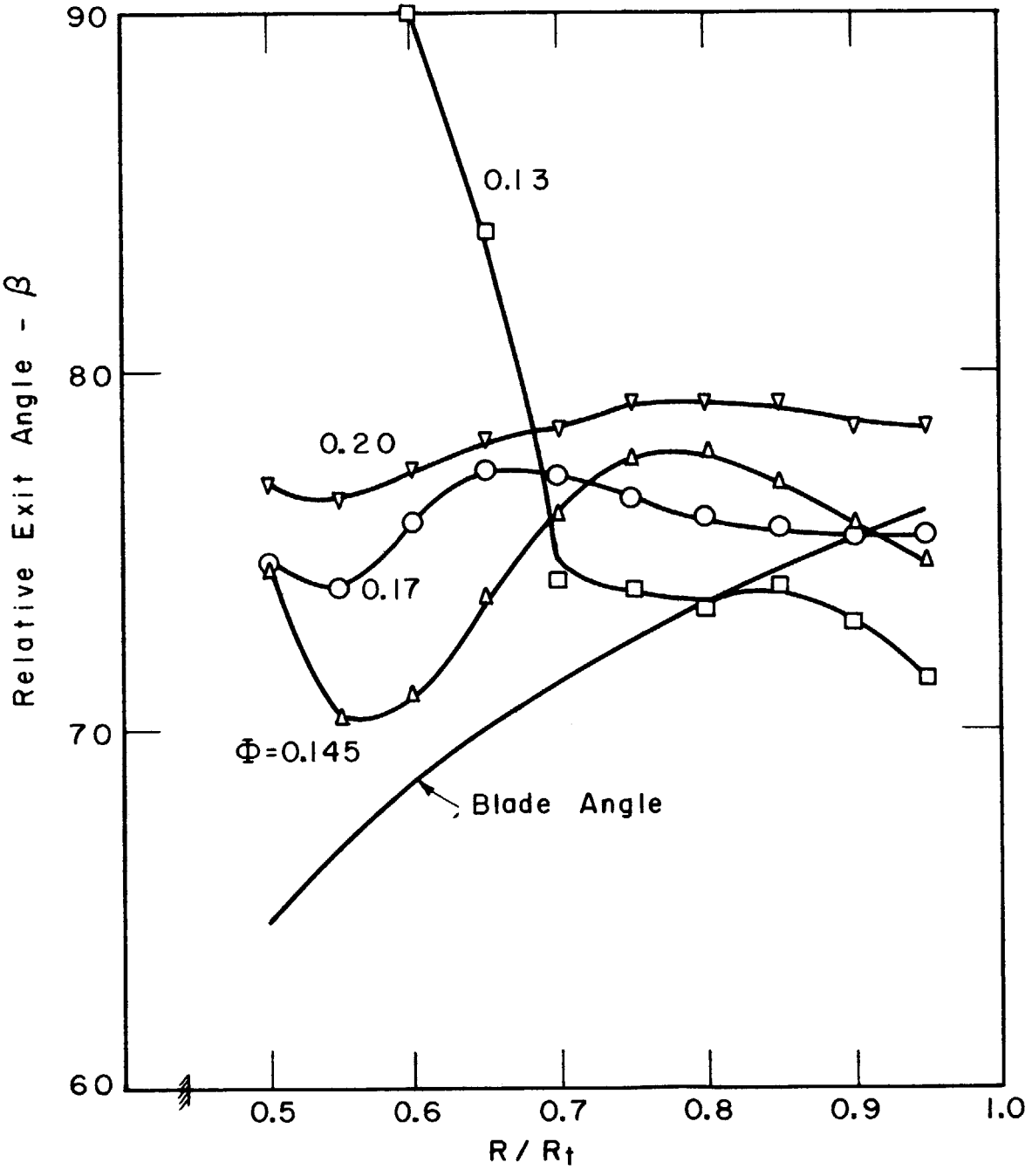

FIG. 16A RELATIVE EXIT ANGLE - FLAT PLATE INDUCER

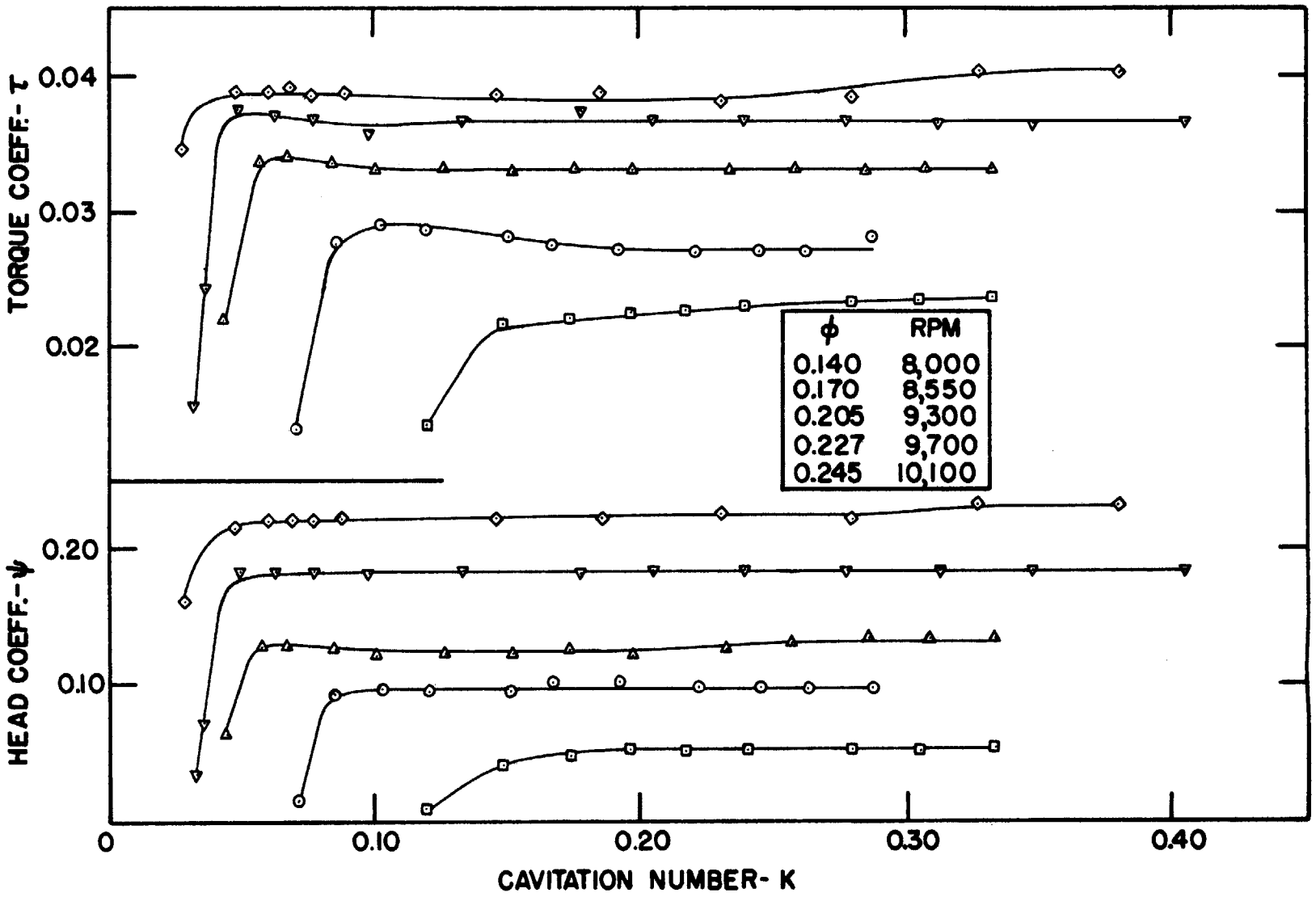

FIG. 17- CAVITATING PERFORMANCE- STENNING'S DESIGN

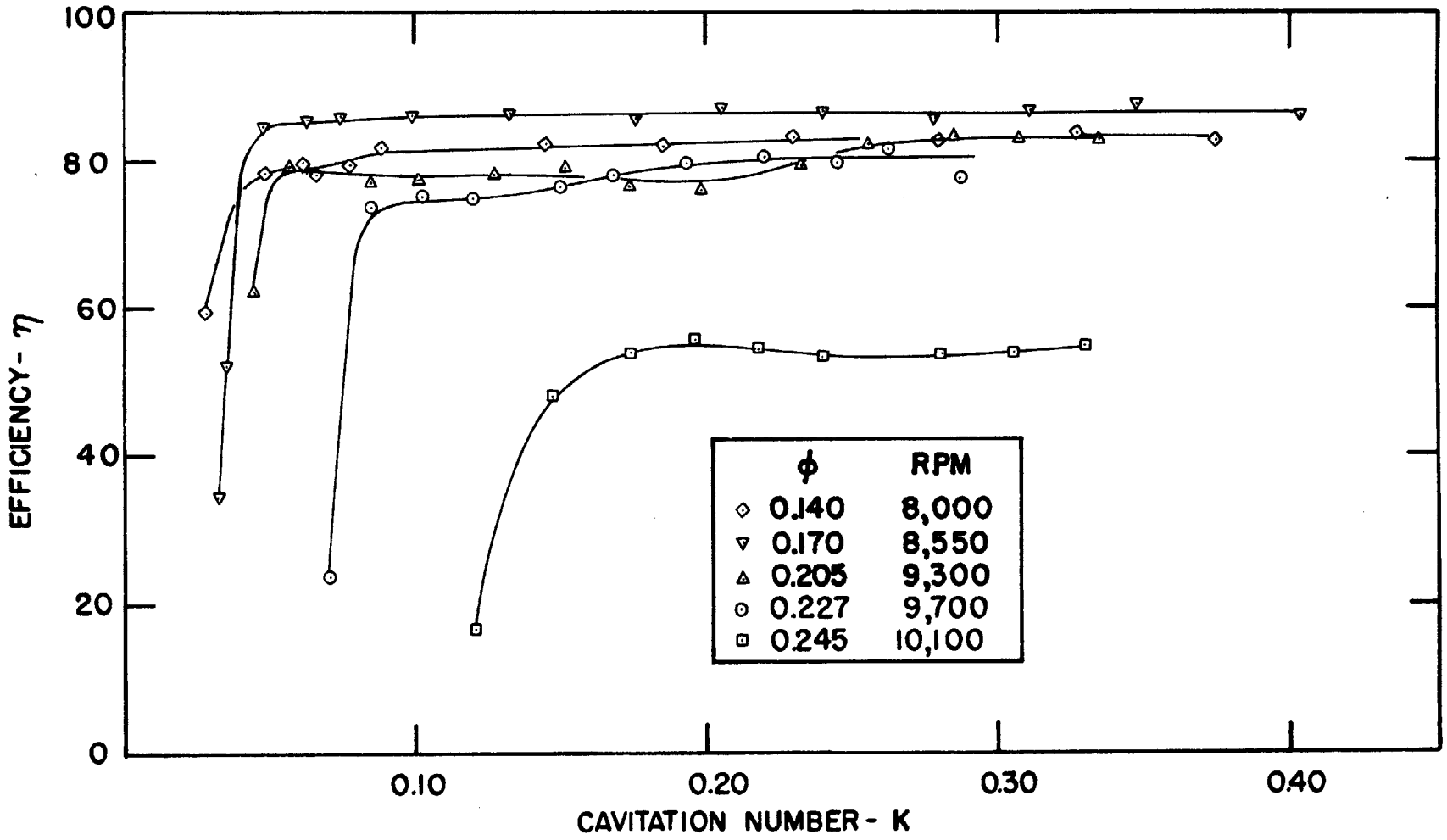

FIG. 18 - CAVITATING PERFORMANCE - STENNINGS DESIGN

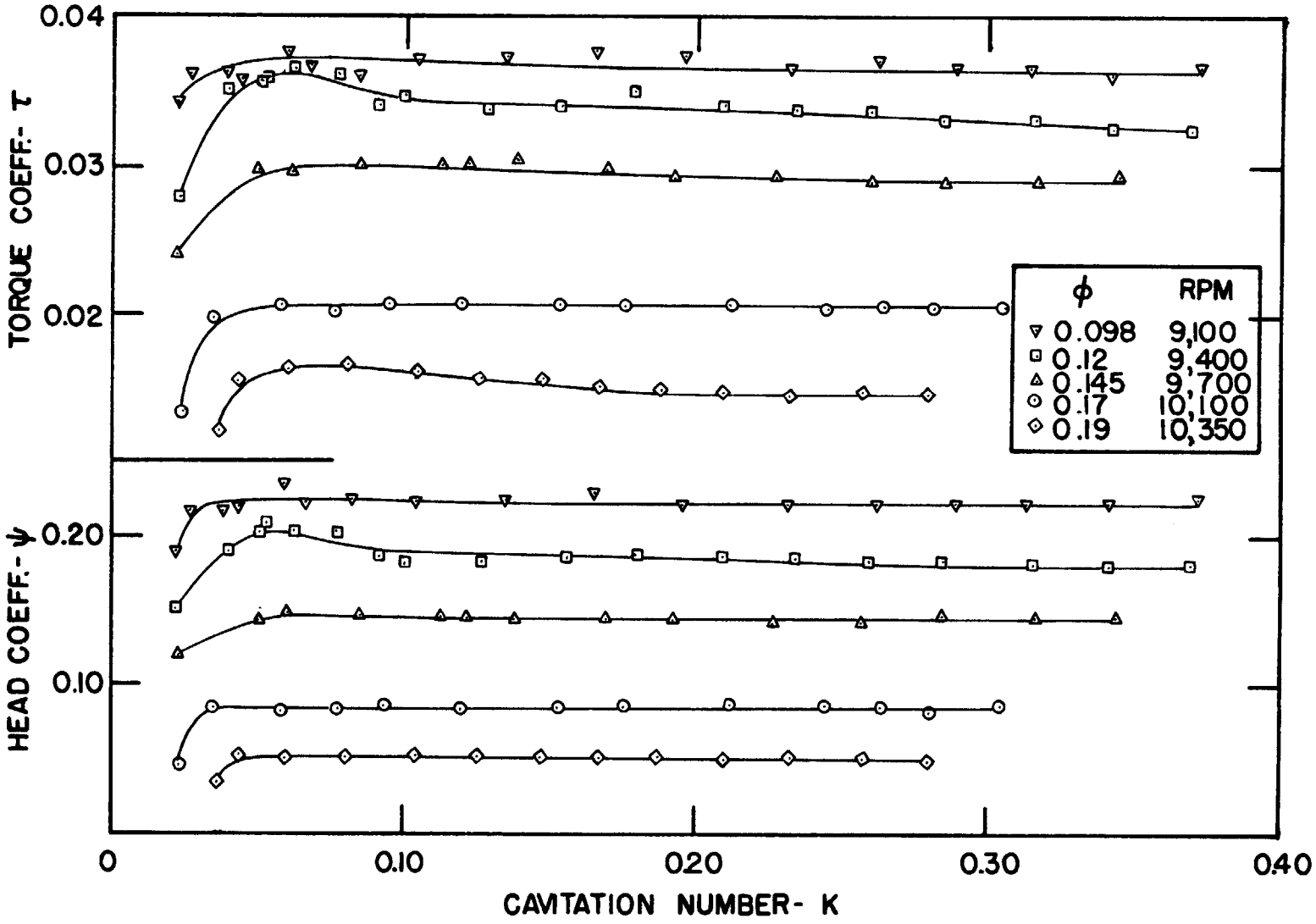

FIG. 19- CAVITATING PERFORMANCE- F.P. INDUCER

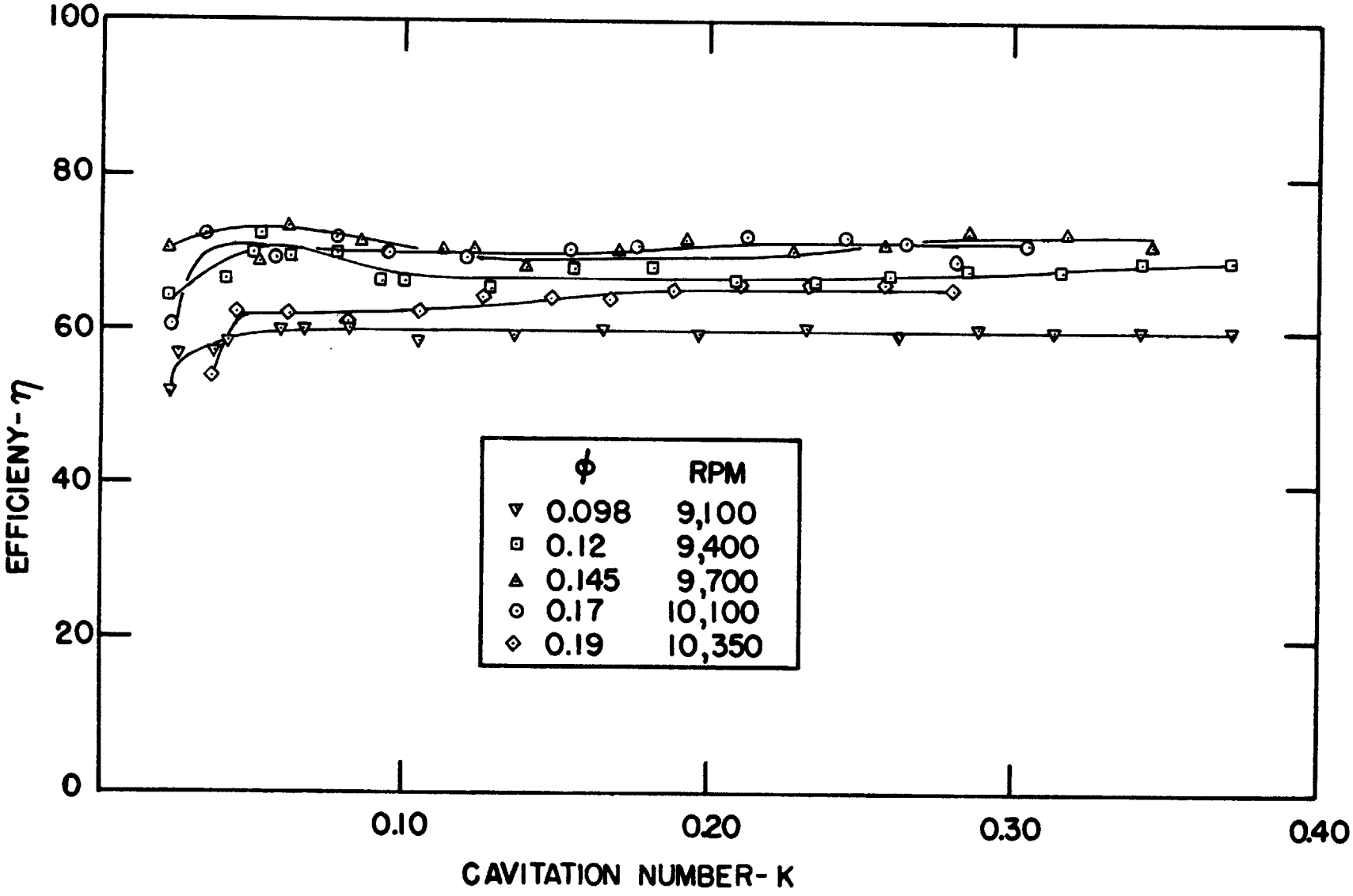

FIG. 20- CAVITATING PERFORMANCE- F.P. INDUCER

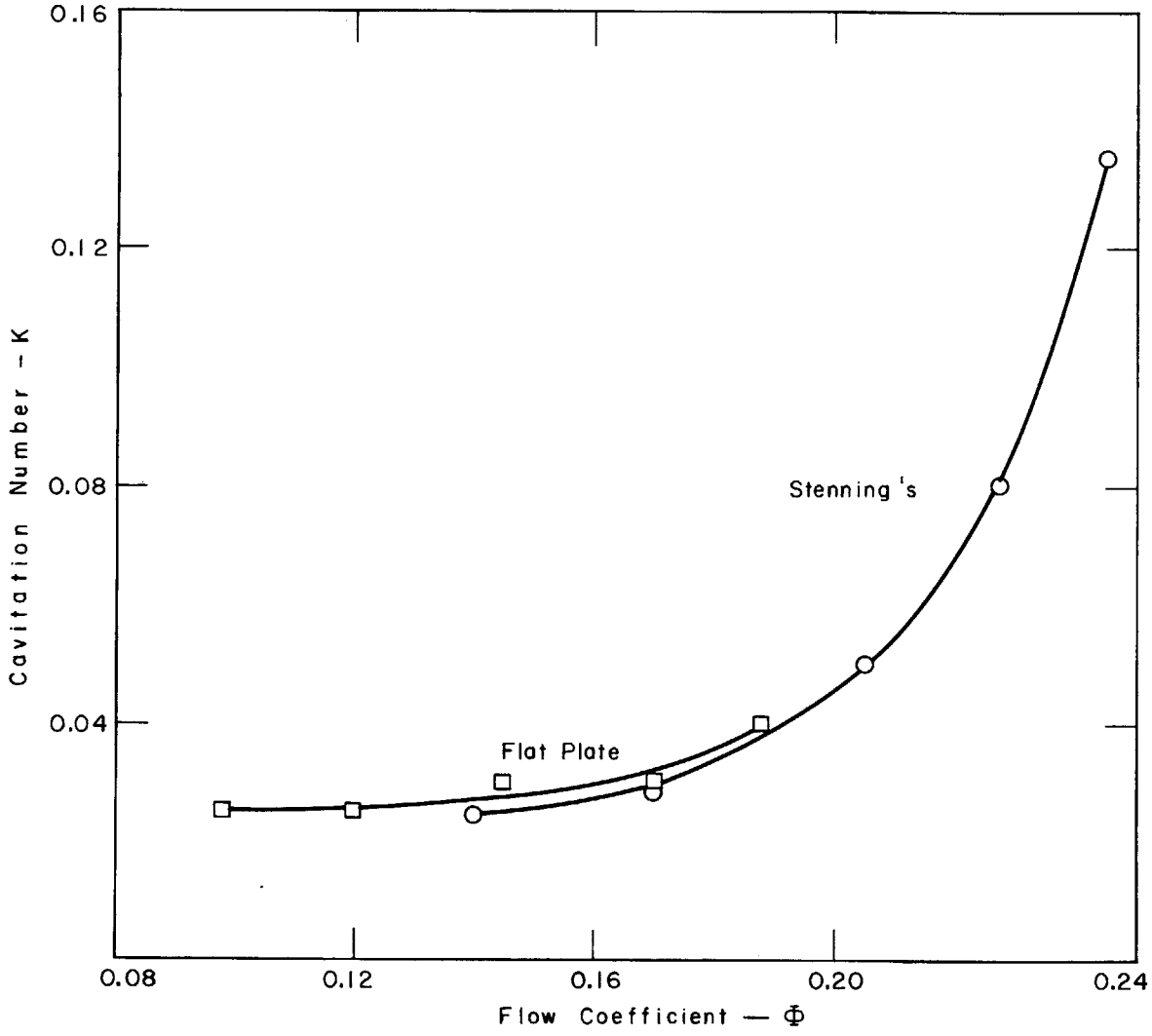

FIG. 21 CAVITATION NUMBER AT BREAKDOWN INCEPTION (90 % NON-CAV. HEAD)

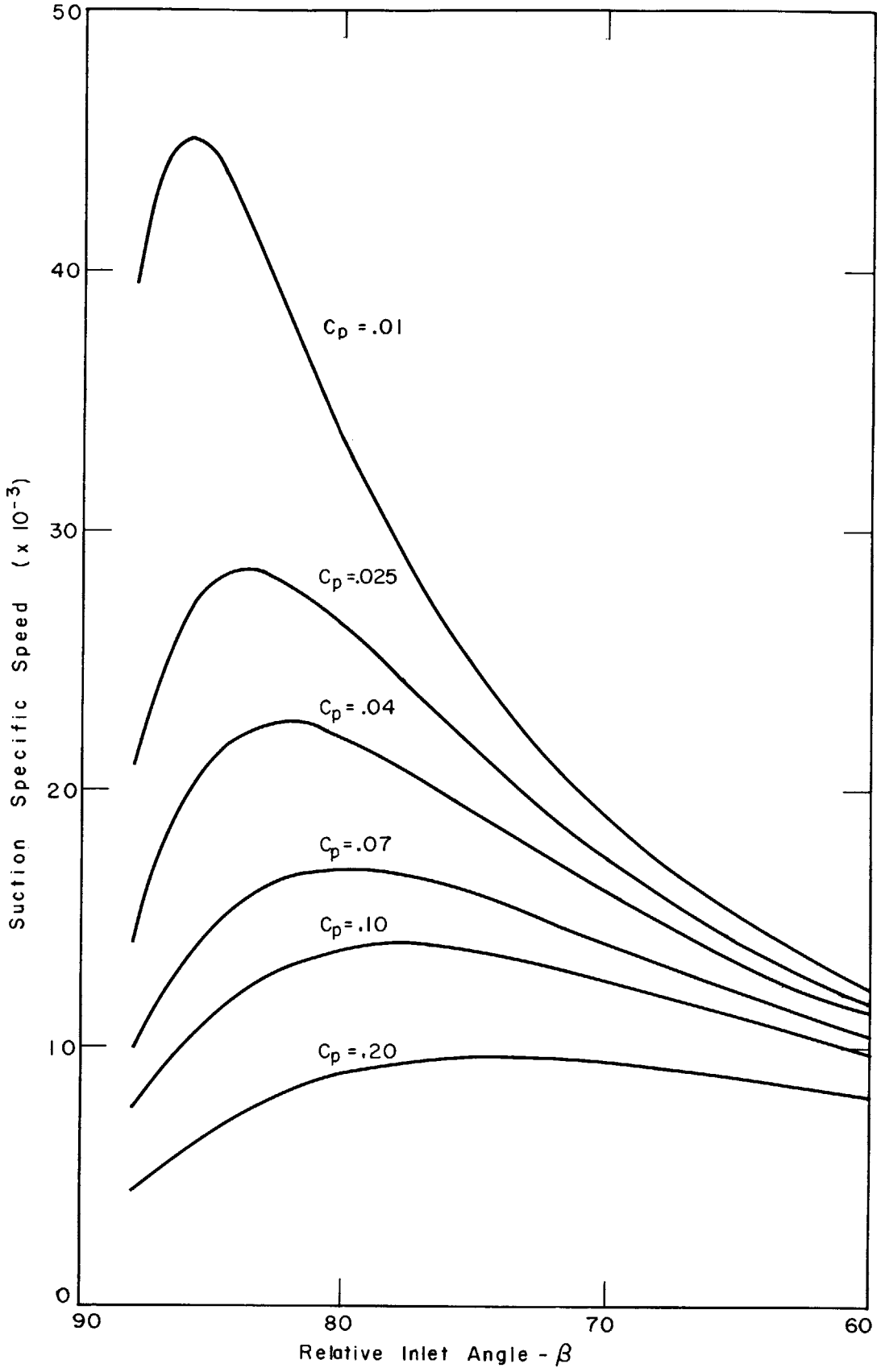

FIG. 22 SUCTION SPECIFIC SPEED VS RELATIVE INLET ANGLE

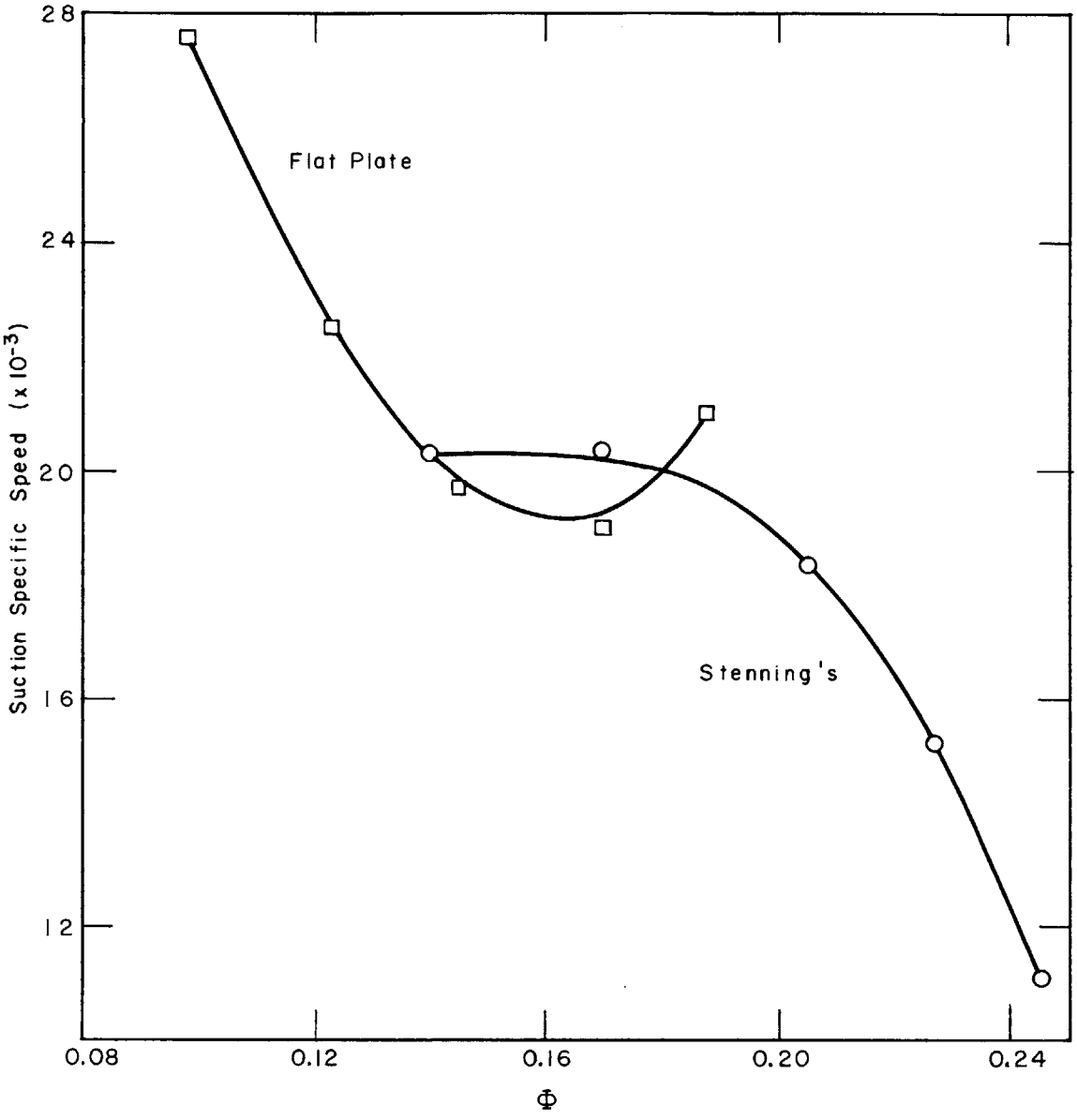

FIG. 23 SUCTION SPECIFIC SPEED AT BREAKDOWN INCEPTION (90 % NON-CAV. HEAD)

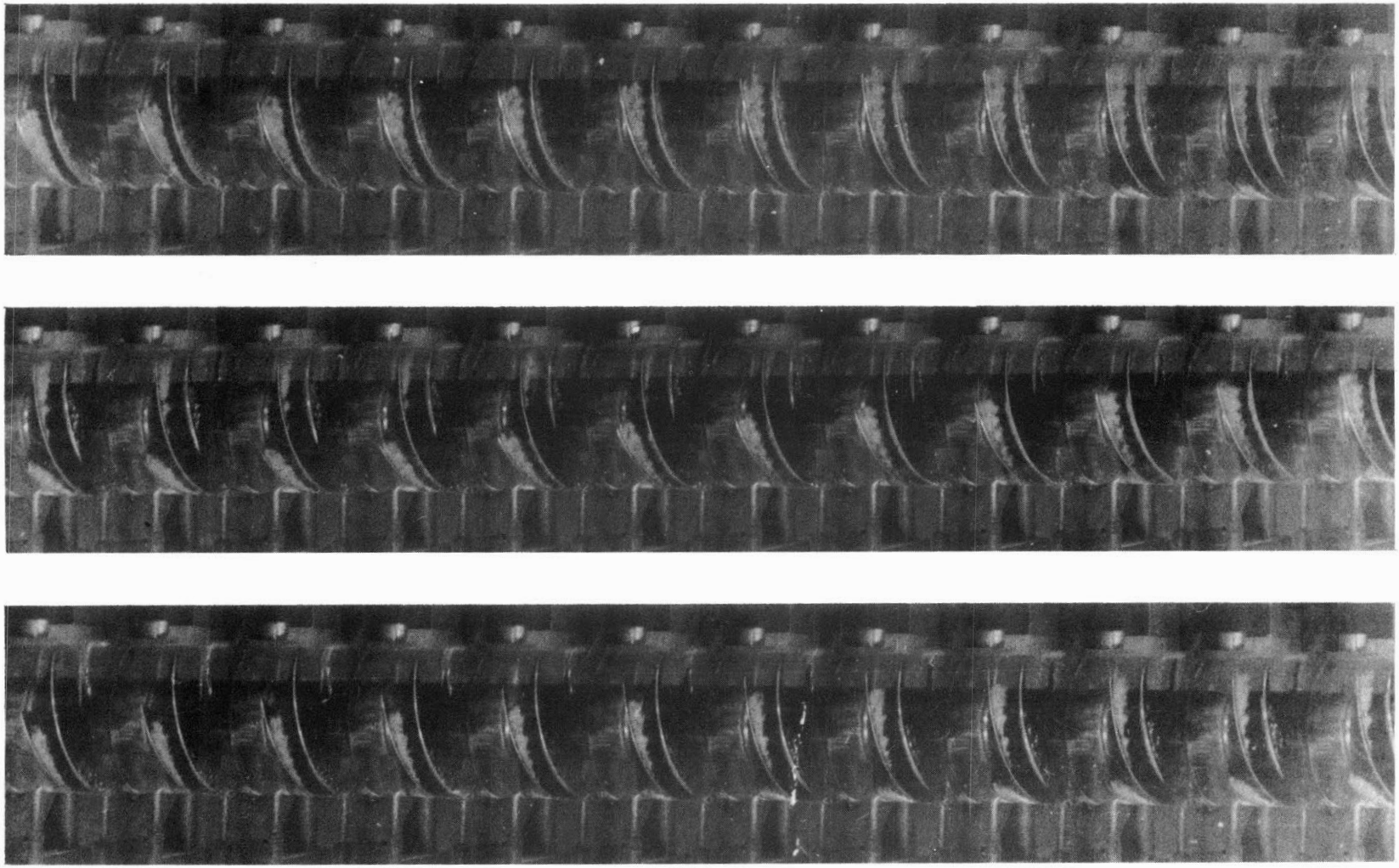

Φ=0.227, K=0.08, 100% NON-CAV. HEAD, 9,700 RPM

FIG. 24A - CAVITATION FORMATION (STENNING)

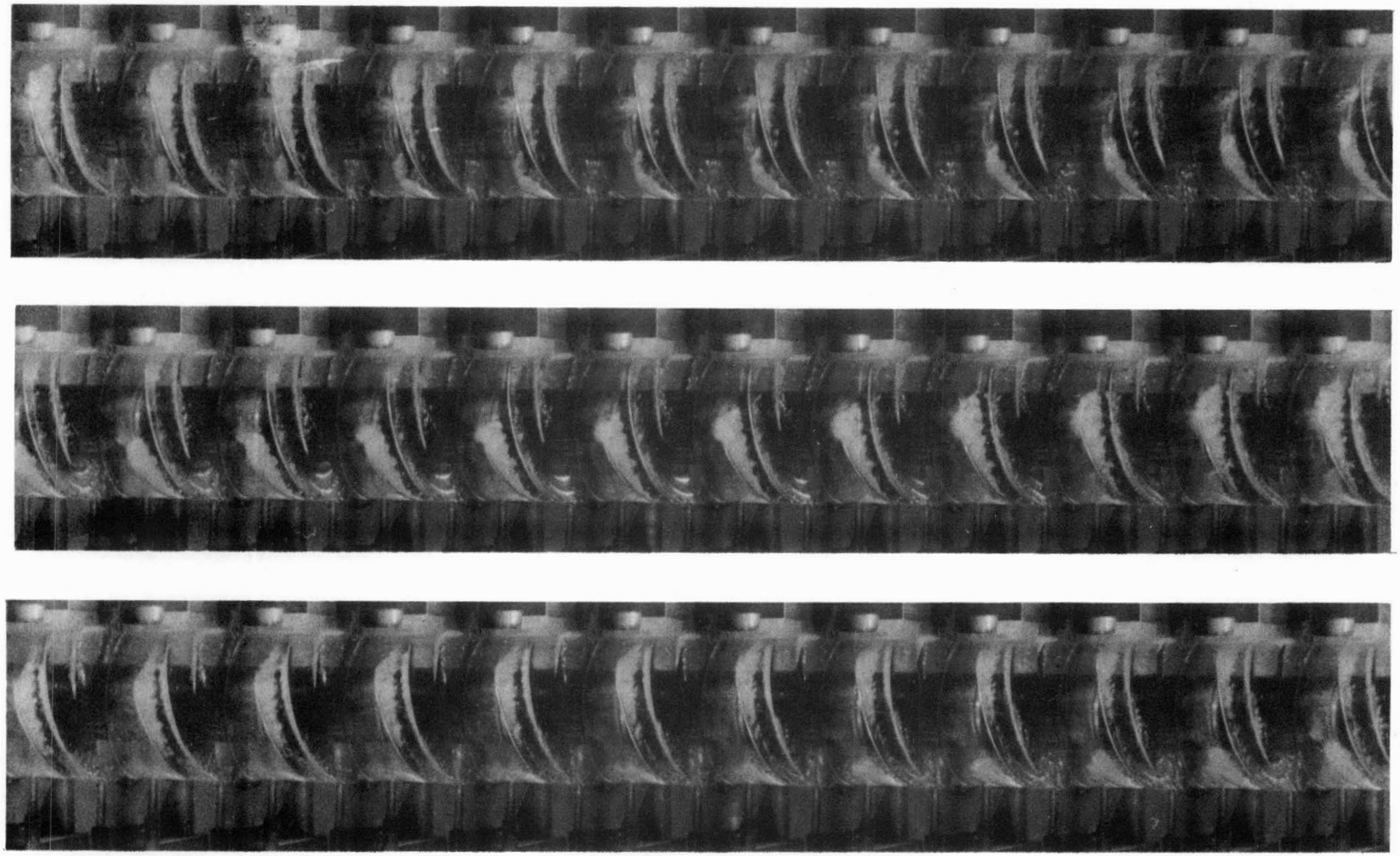

Φ=0.227, K=0.07, 40% NON-CAV. HEAD, 9,700RPM

FIG. 24B - CAVITATION FORMATION

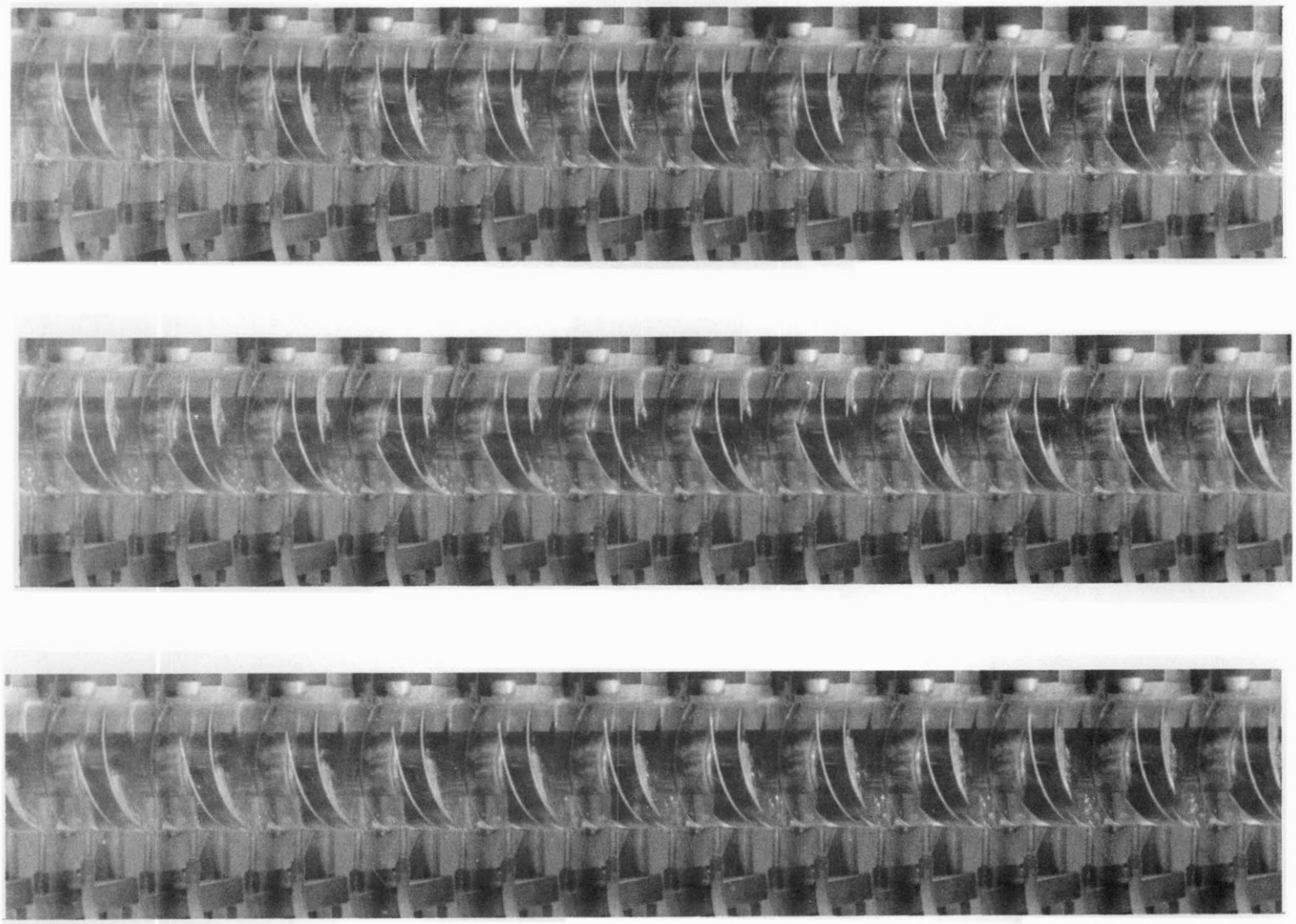

$\Phi = 0.20$, $K = 0.11$, 100% NON-CAV. HEAD, 9,300 RPM

FIG. 25A - CAVITATION FORMATION (STENNING)

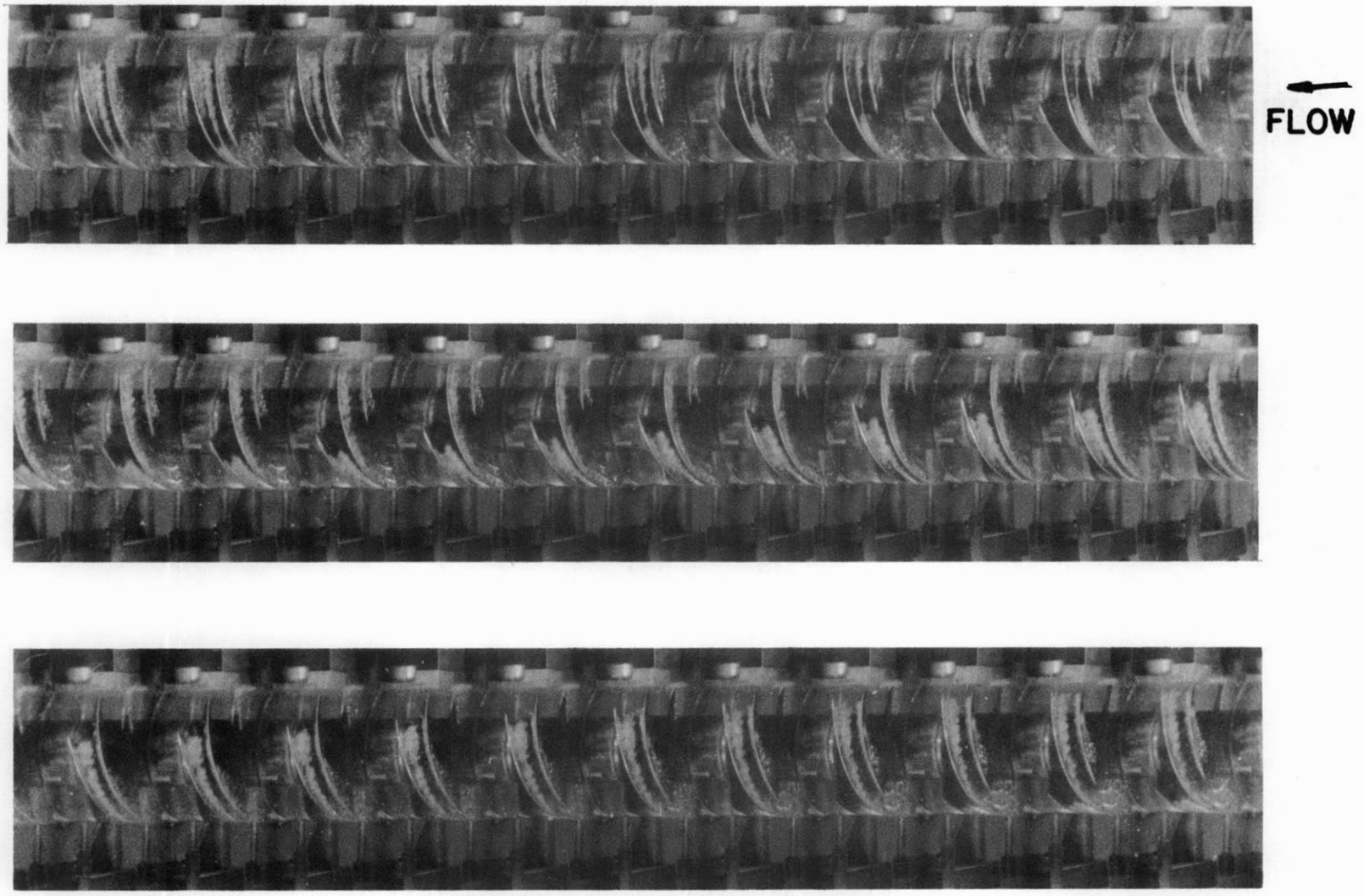

Φ=0.20, K=0.06, 100% NON-CAV. HEAD, 9,300RPM

FIG.25 B - CAVITATION FORMATION

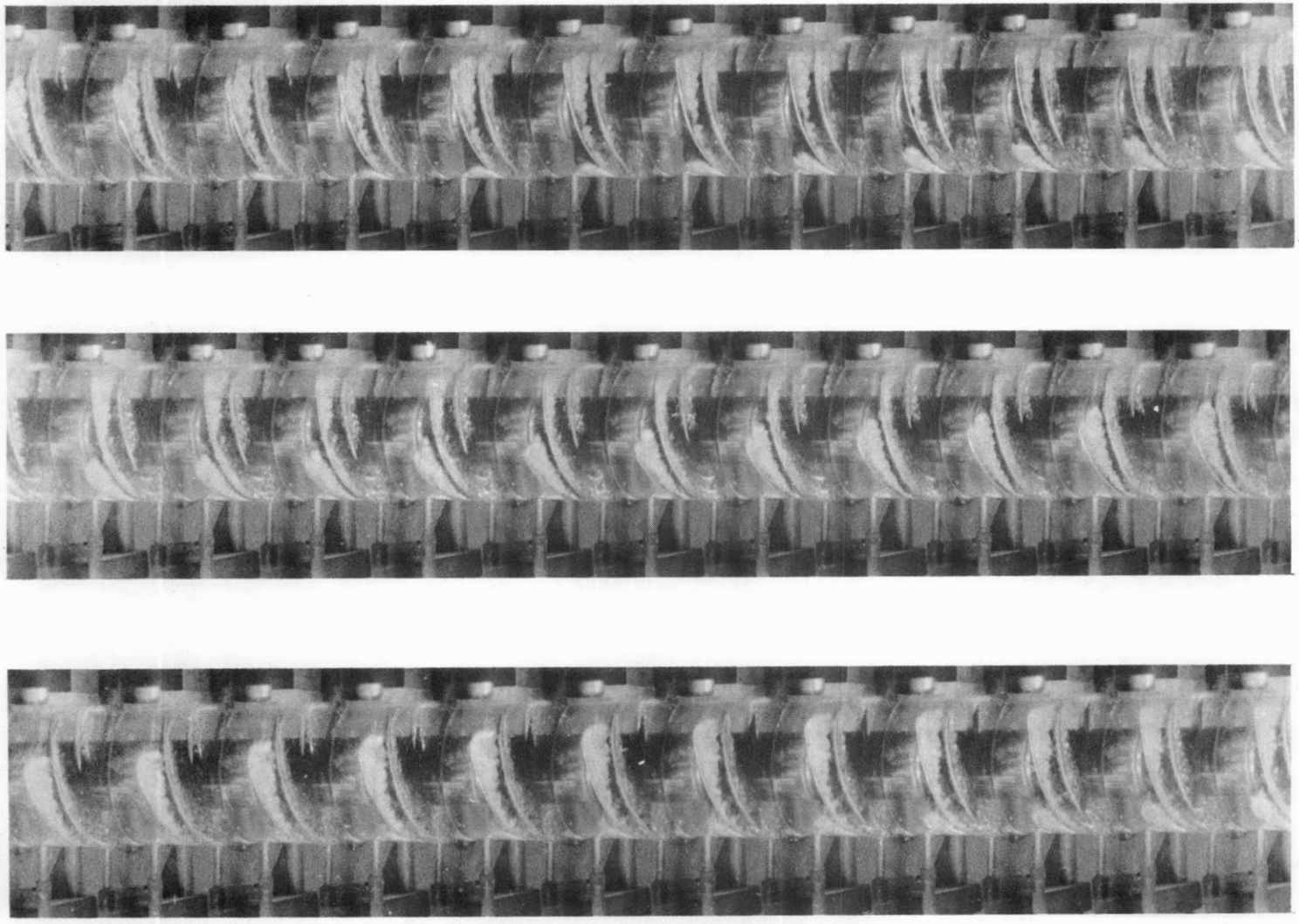

Φ=0.20, K=0.04, 40% NON-CAV. HEAD, 9,300 RPM

FIG. 25C - CAVITATION FORMATION

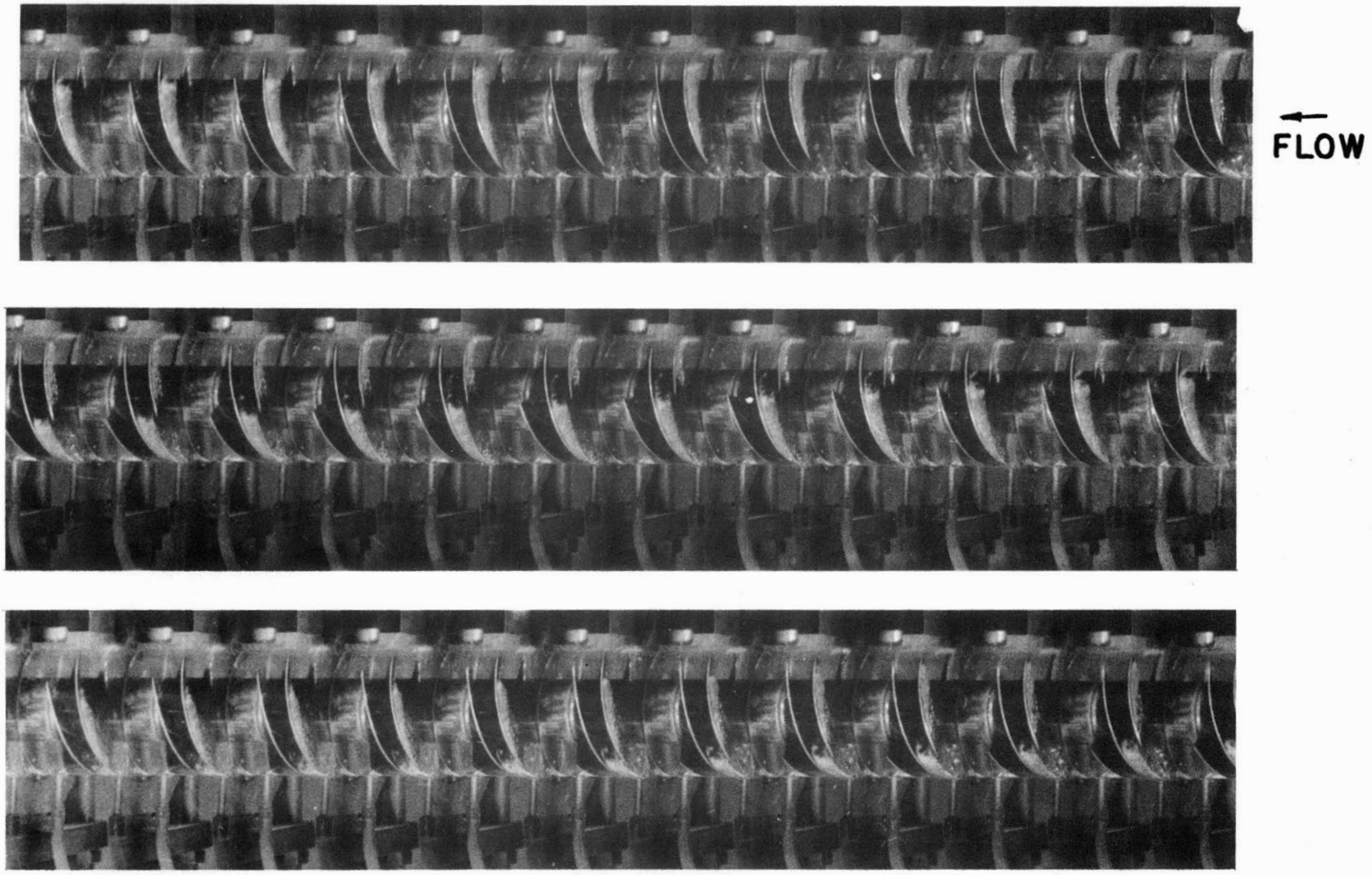

Φ=0.17, K=0.08, 100% NON-CAV. HEAD, 8,550 RPM

FIG. 26A - CAVITATION FORMATION (STENNING)

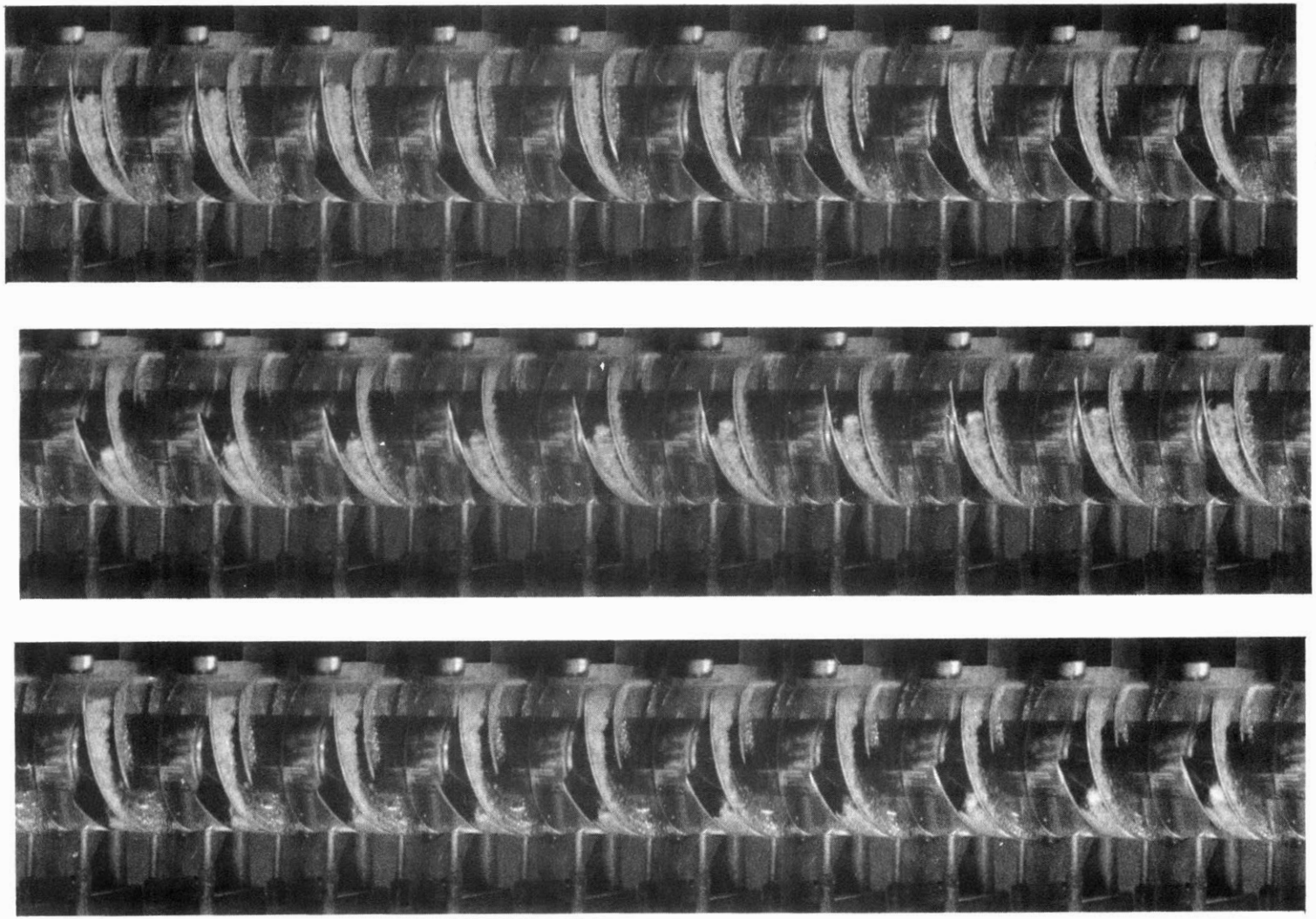

Φ=0.17, K=0.04, 75% NON-CAV. HEAD, 8,550 RPM

FIG. 26B - CAVITATION FORMATION

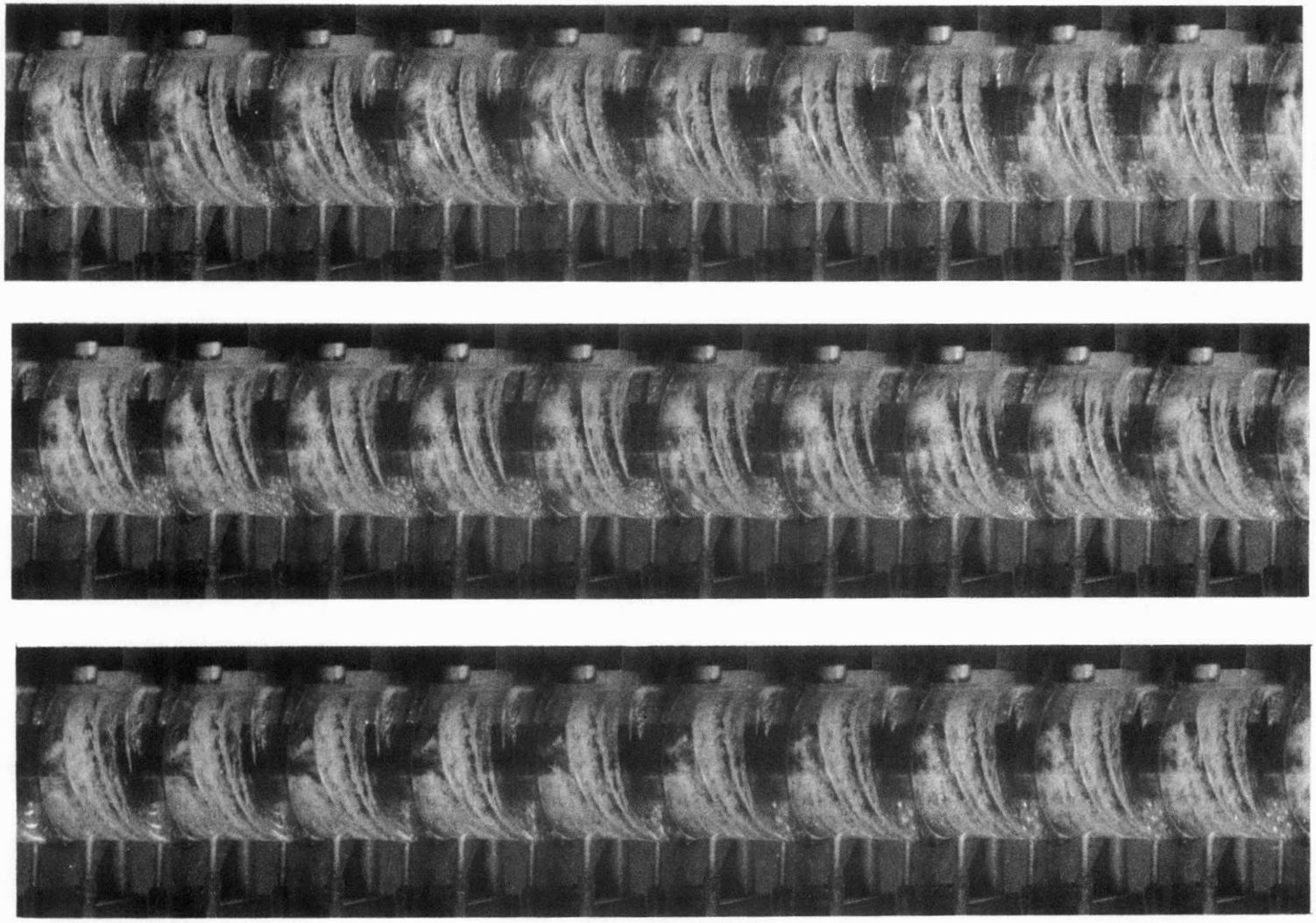

$\Phi = 0.17$, $K = 0.03$, 10% NON-CAV. HEAD, 8,550 RPM

FIG. 26C - CAVITATION FORMATION

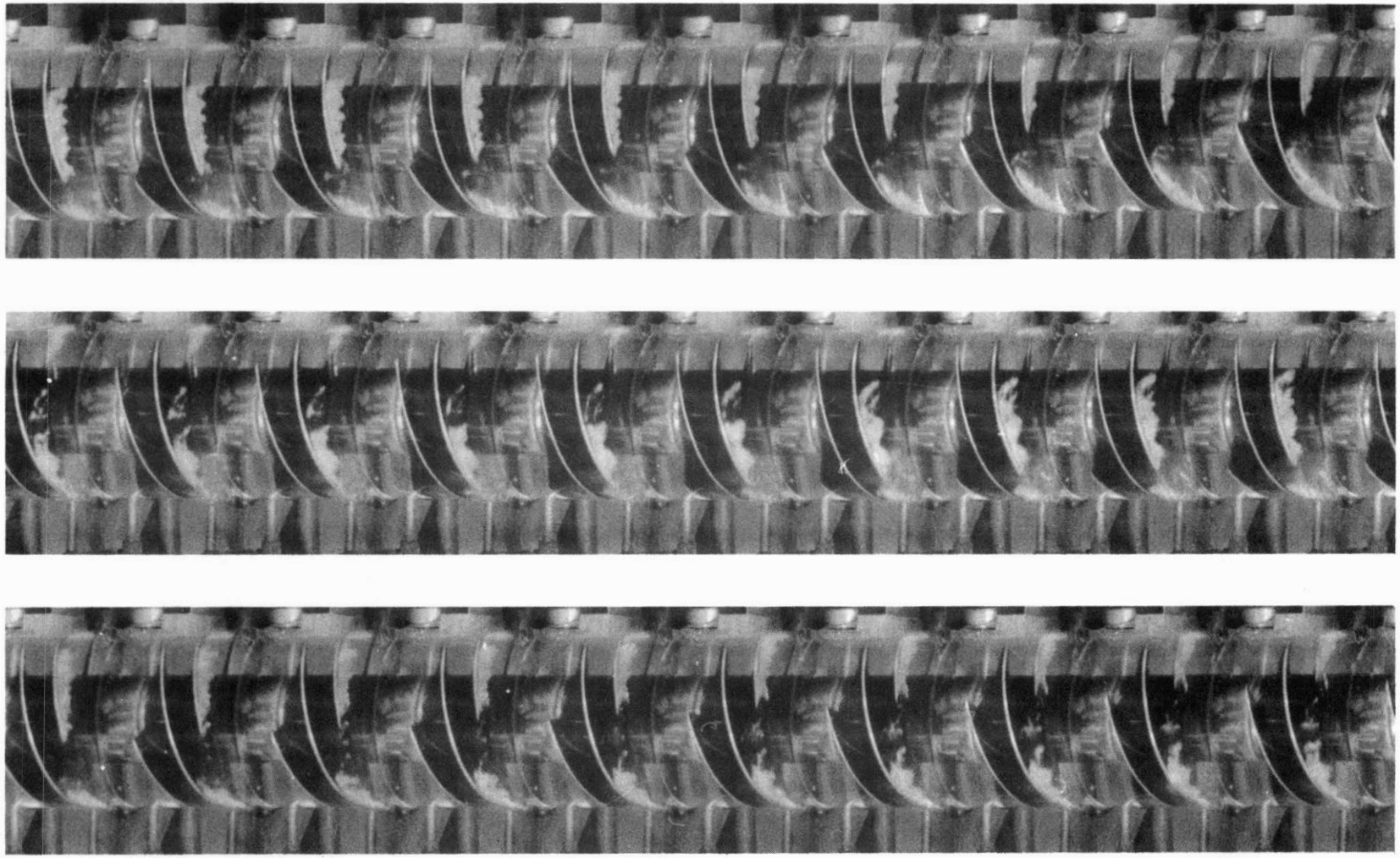

Φ=0.14, K=0.15, 100% NON-CAV. HEAD, 8,000RPM

FIG. 27A- CAVITATION FORMATION (STENNING)

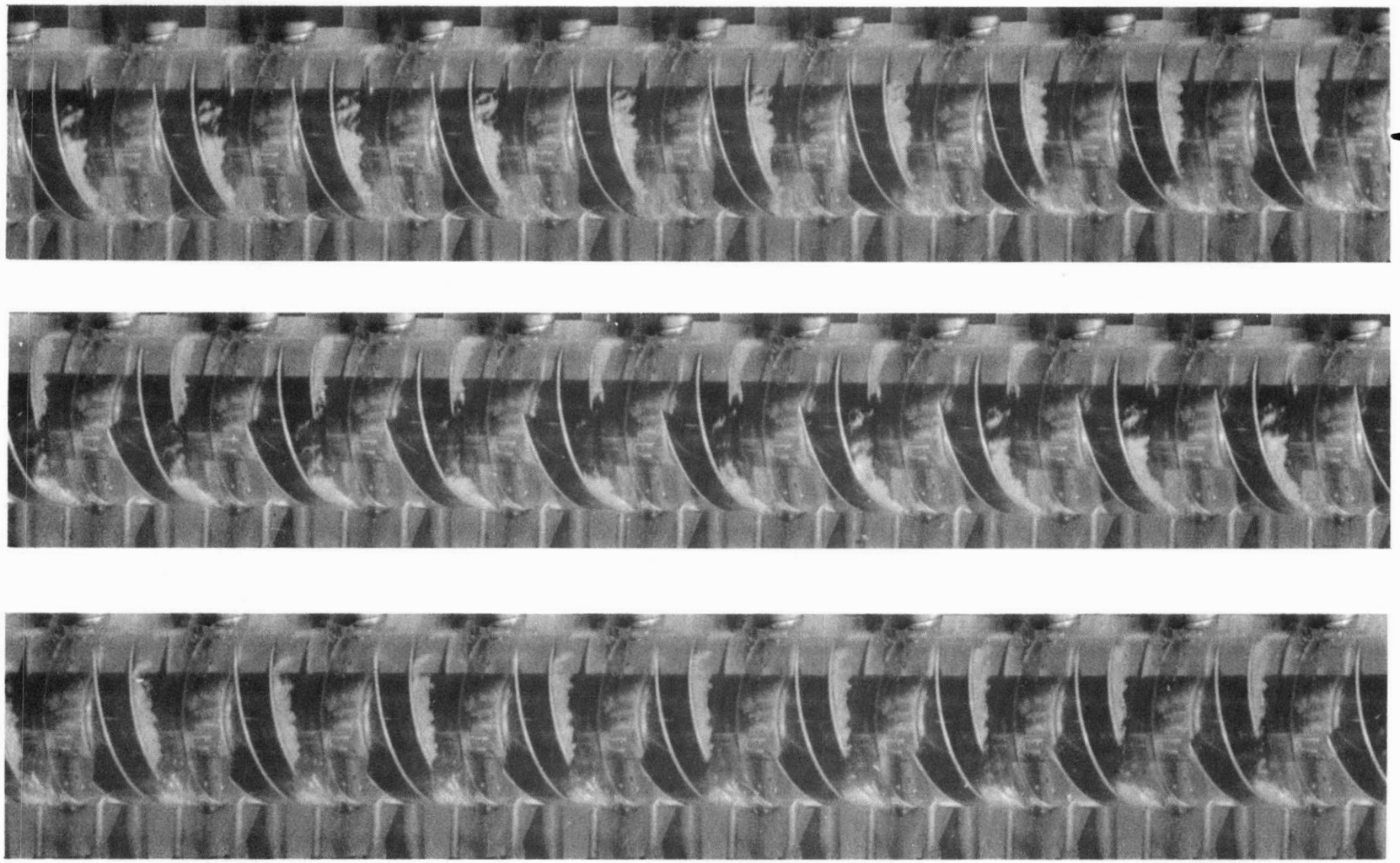

Φ=0.14, K=0.09, 100% NON-CAV. HEAD, 8,000RPM

FIG.27B-CAVITATION FORMATION

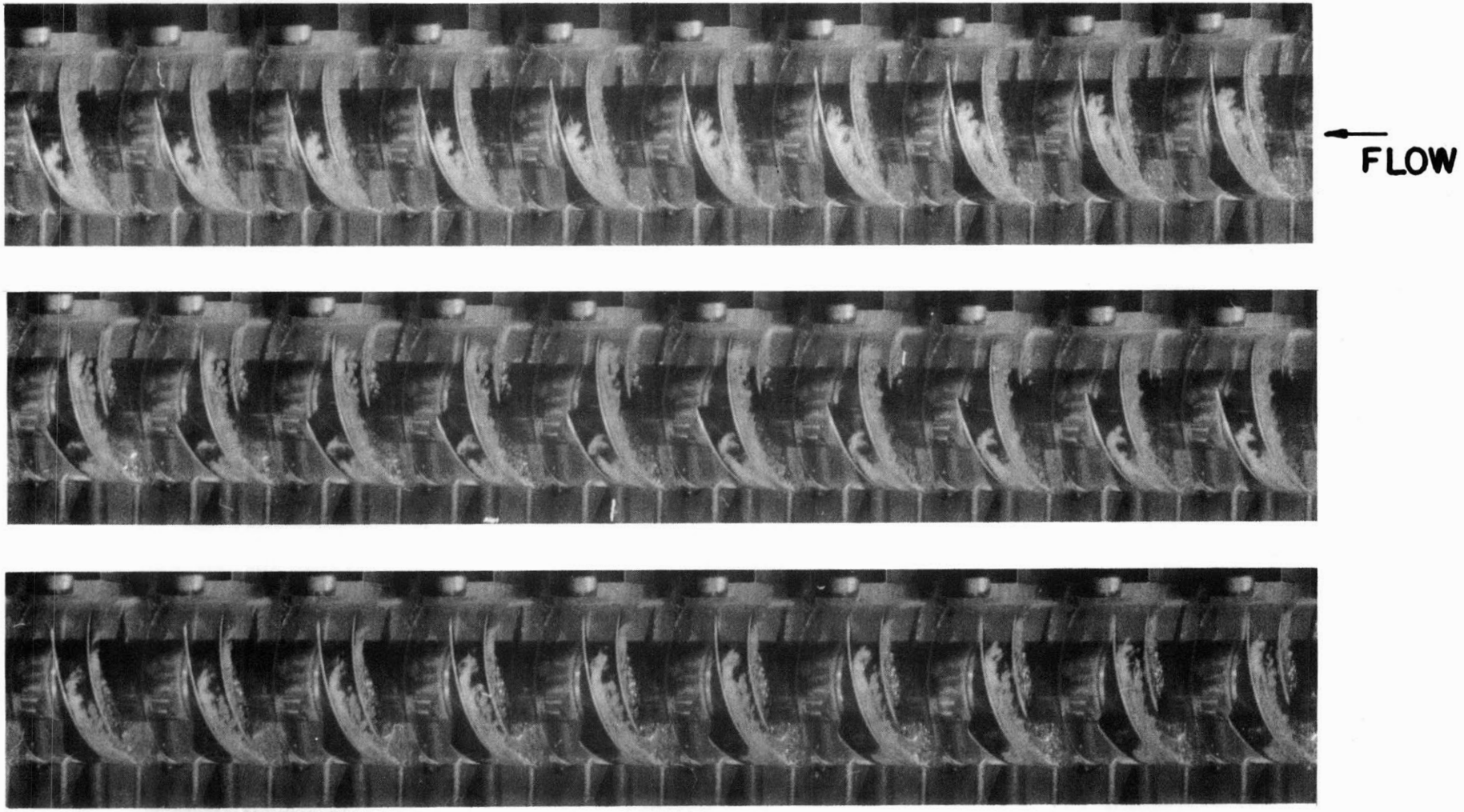

Φ=0.14, K=0.05, 95% NON-CAV. HEAD, 8,000 RPM

FIG. 27C- CAVITATION FORMATION

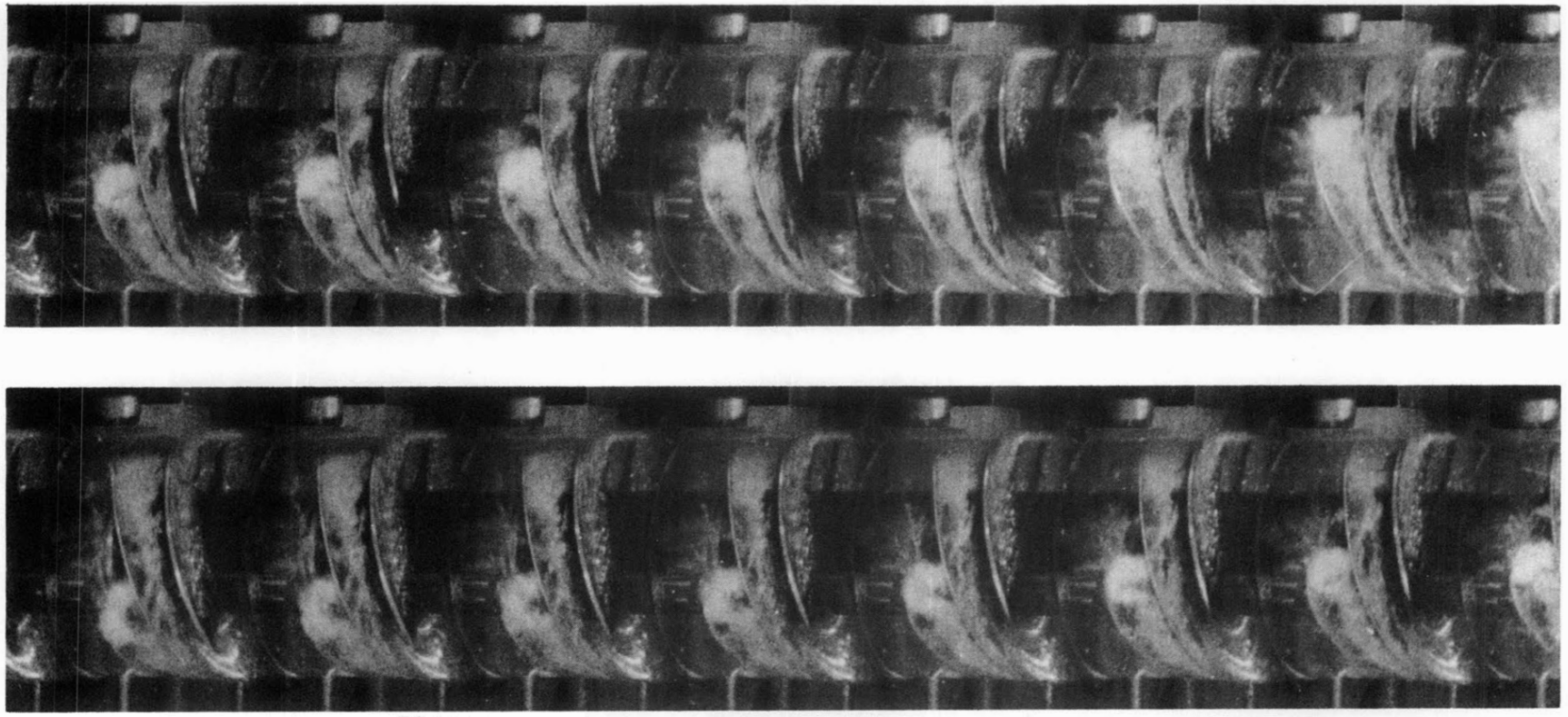

Φ=0.14, K=0.02, 50% NON-CAV. HEAD, 8,000 RPM

FIG. 27D- CAVITATION FORMATION

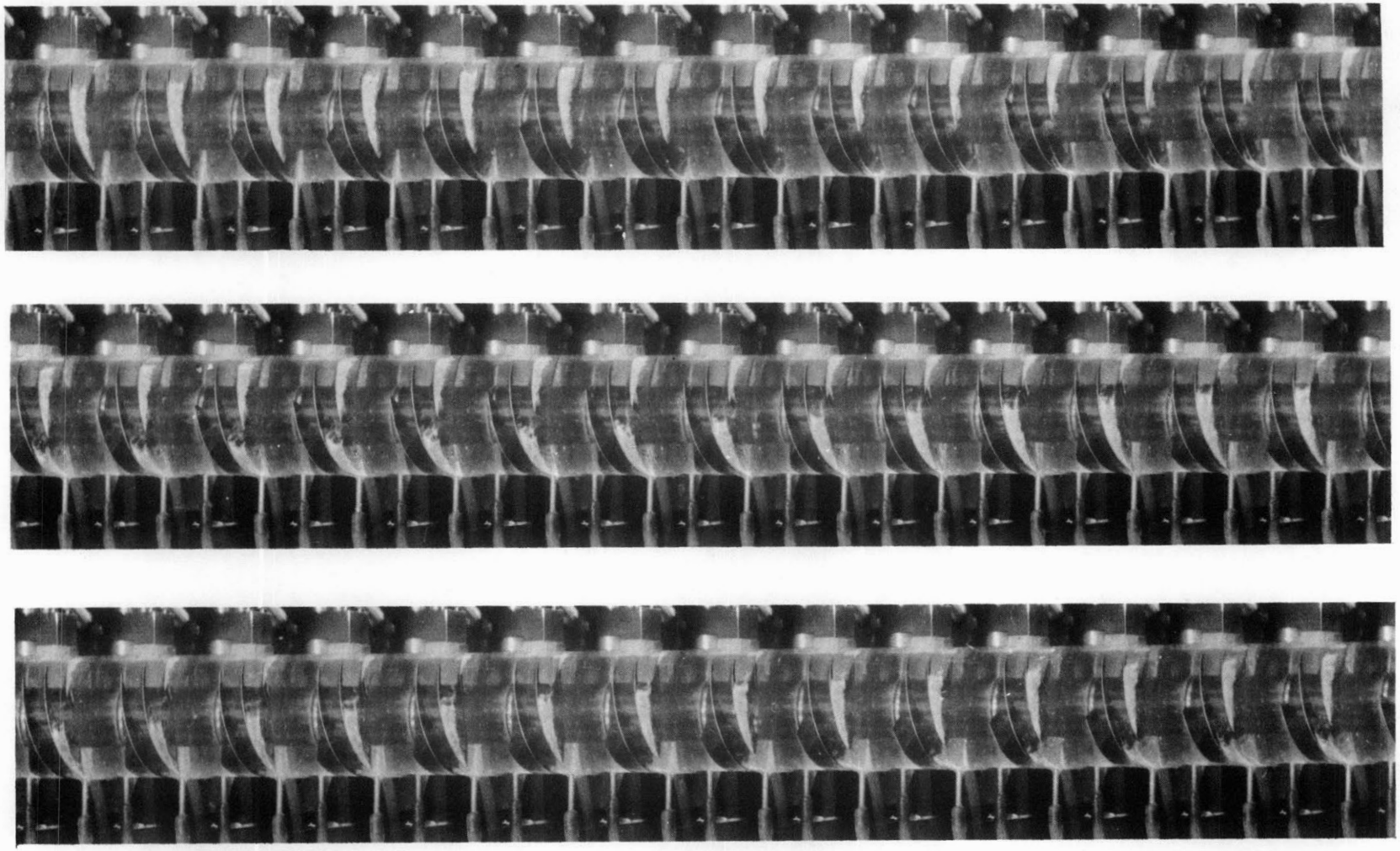

$\Phi = 0.17,\ K = 0.12,\ 10{,}100\ \text{RPM}$

FIG. 28A- CAVITATION FORMATION (F.P. INDUCER)

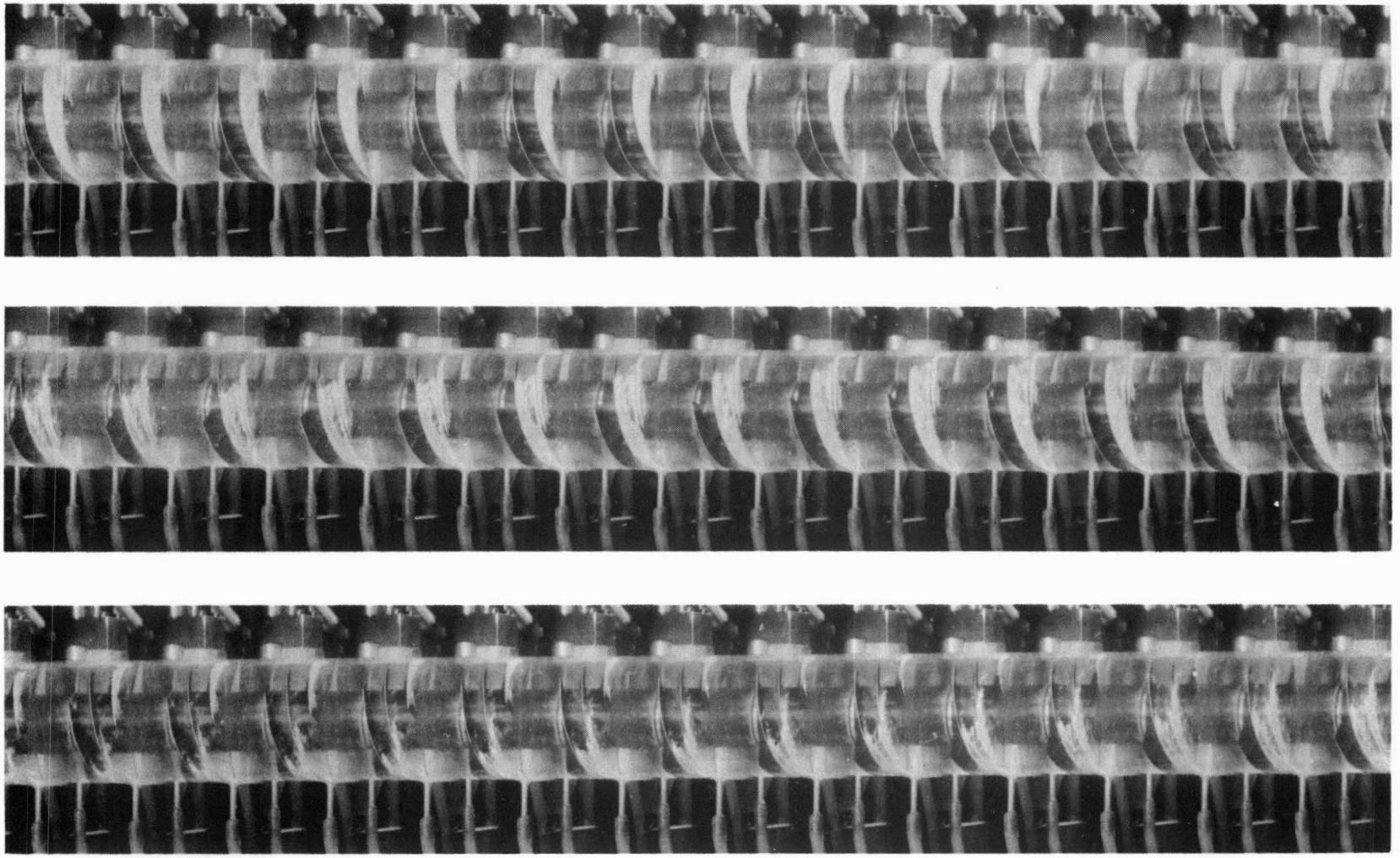

Φ= 0.17, K=0.08, 10,100 RPM

FIG. 28B- CAVITATION FORMATION

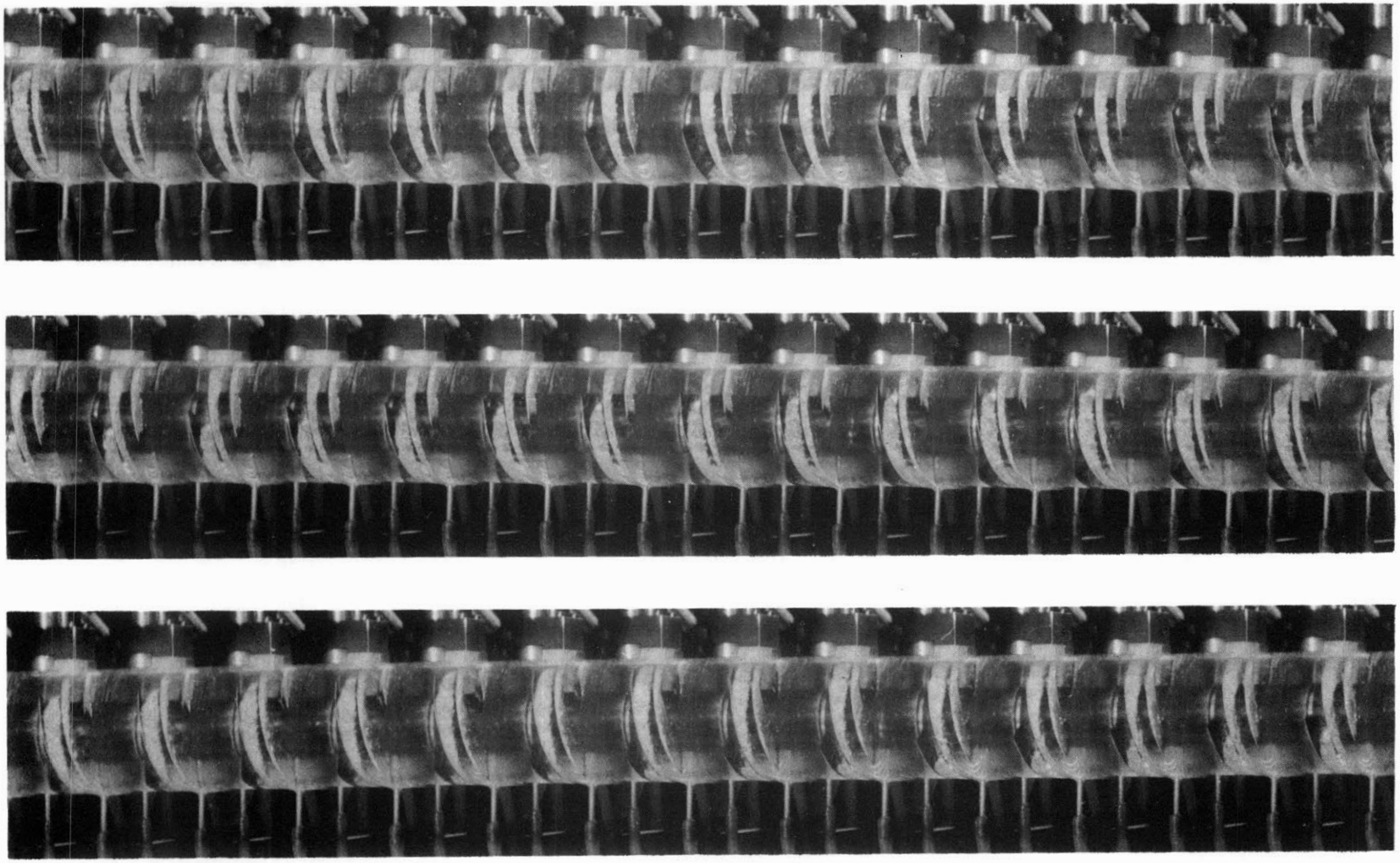

$\Phi = 0.17$, $K = 0.038$, 10,100 RPM

FIG. 28C - CAVITATION FORMATION

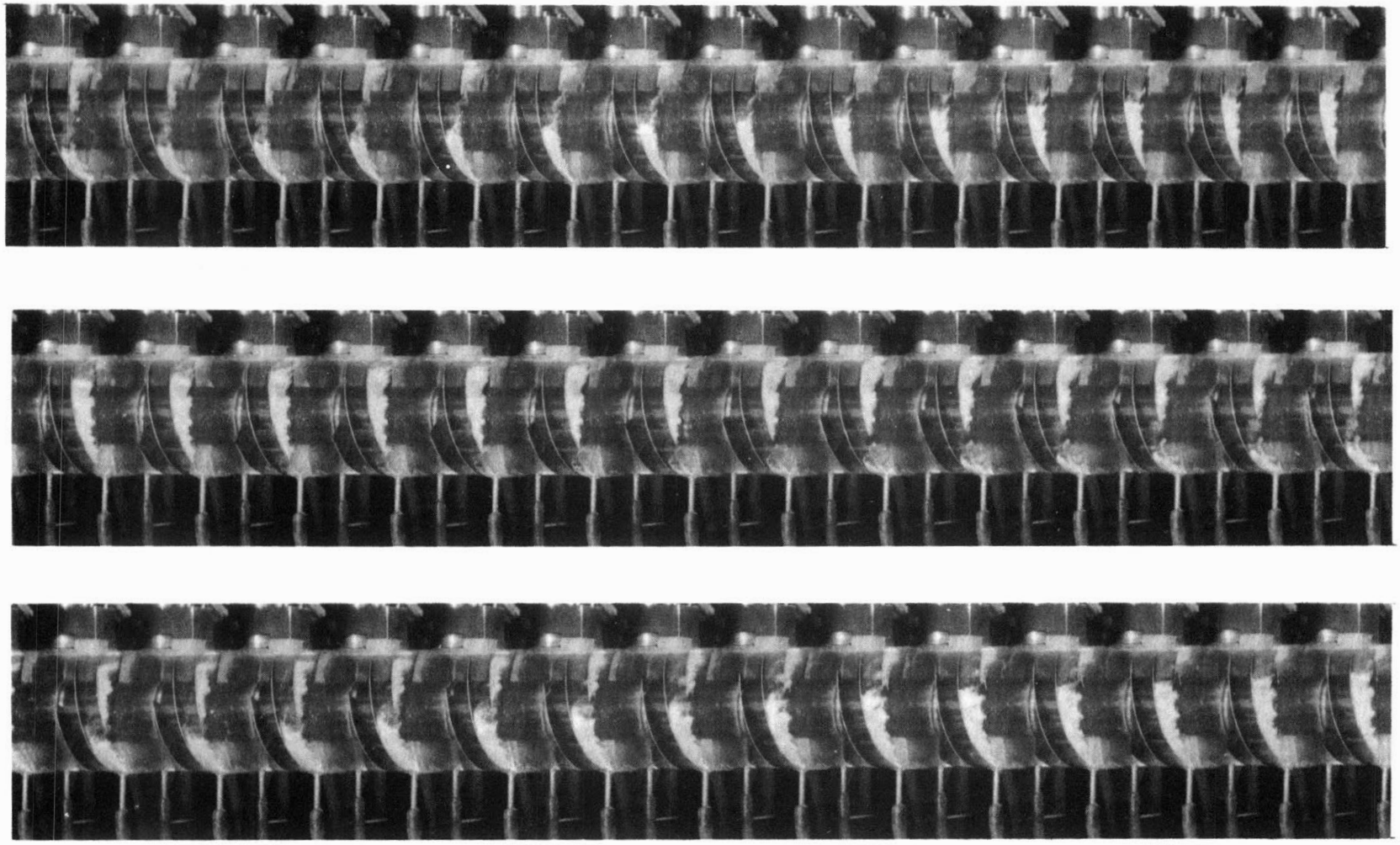

Φ=0.145, K=0.11, 9,700 RPM

FIG. 29A-CAVITATION FORMATION (F.P. INDUCER)

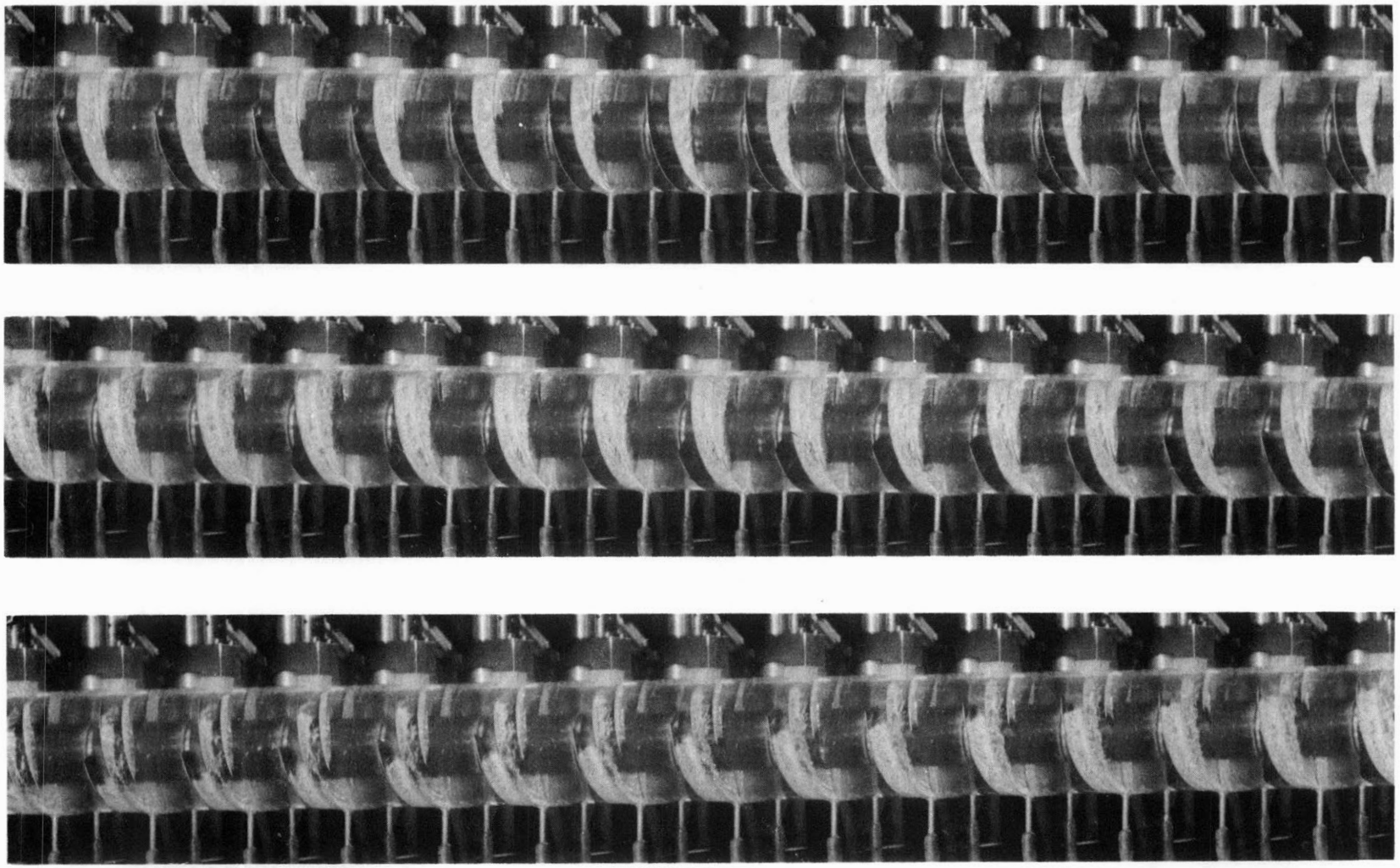

$\Phi = 0.145$, $K = 0.065$, 9,700 RPM

FIG. 29B- CAVITATION FORMATION

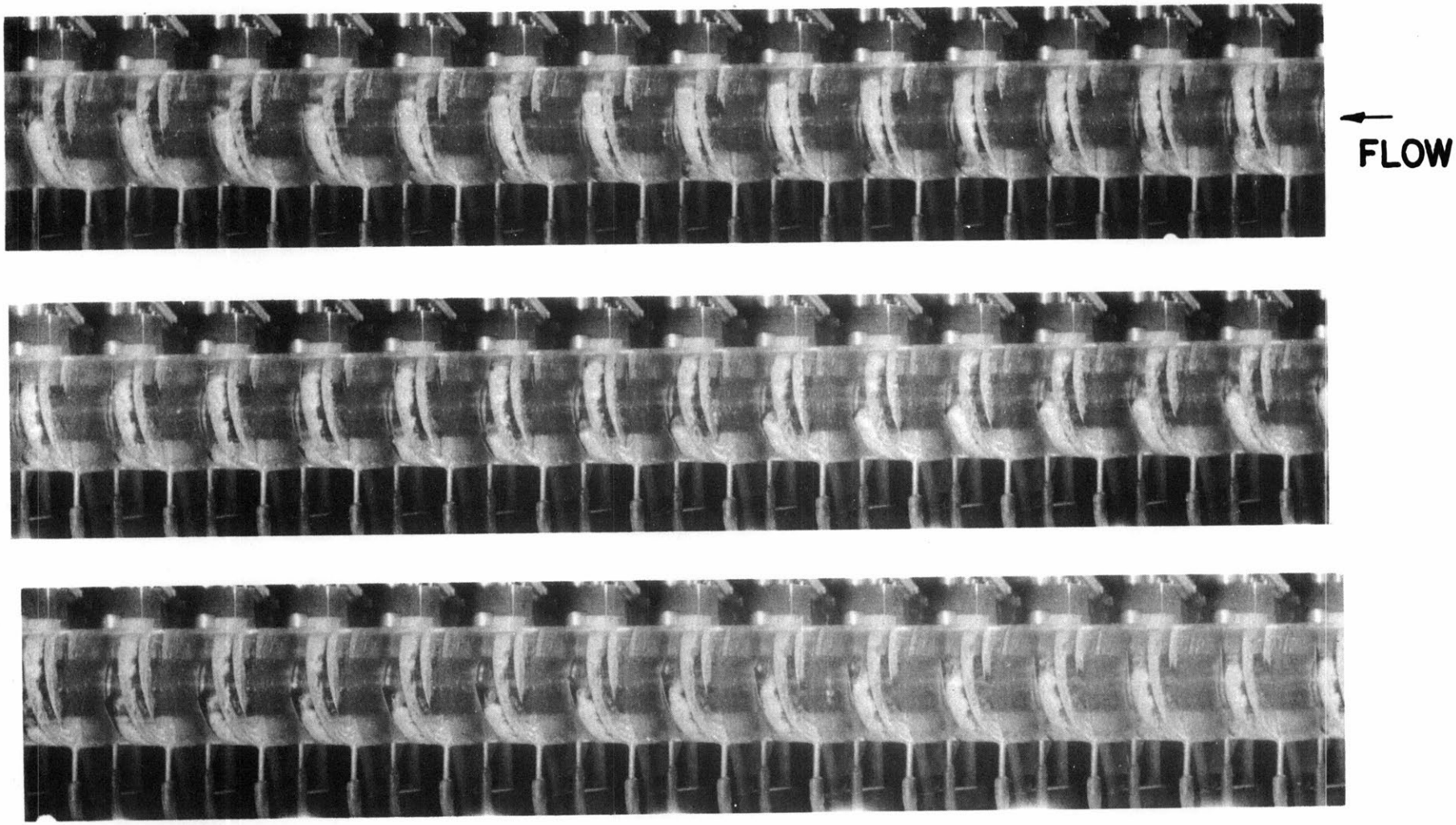

$\Phi = 0.145$, $K = 0.028$, 9,700 RPM

FIG. 29C - CAVITATION FORMATION

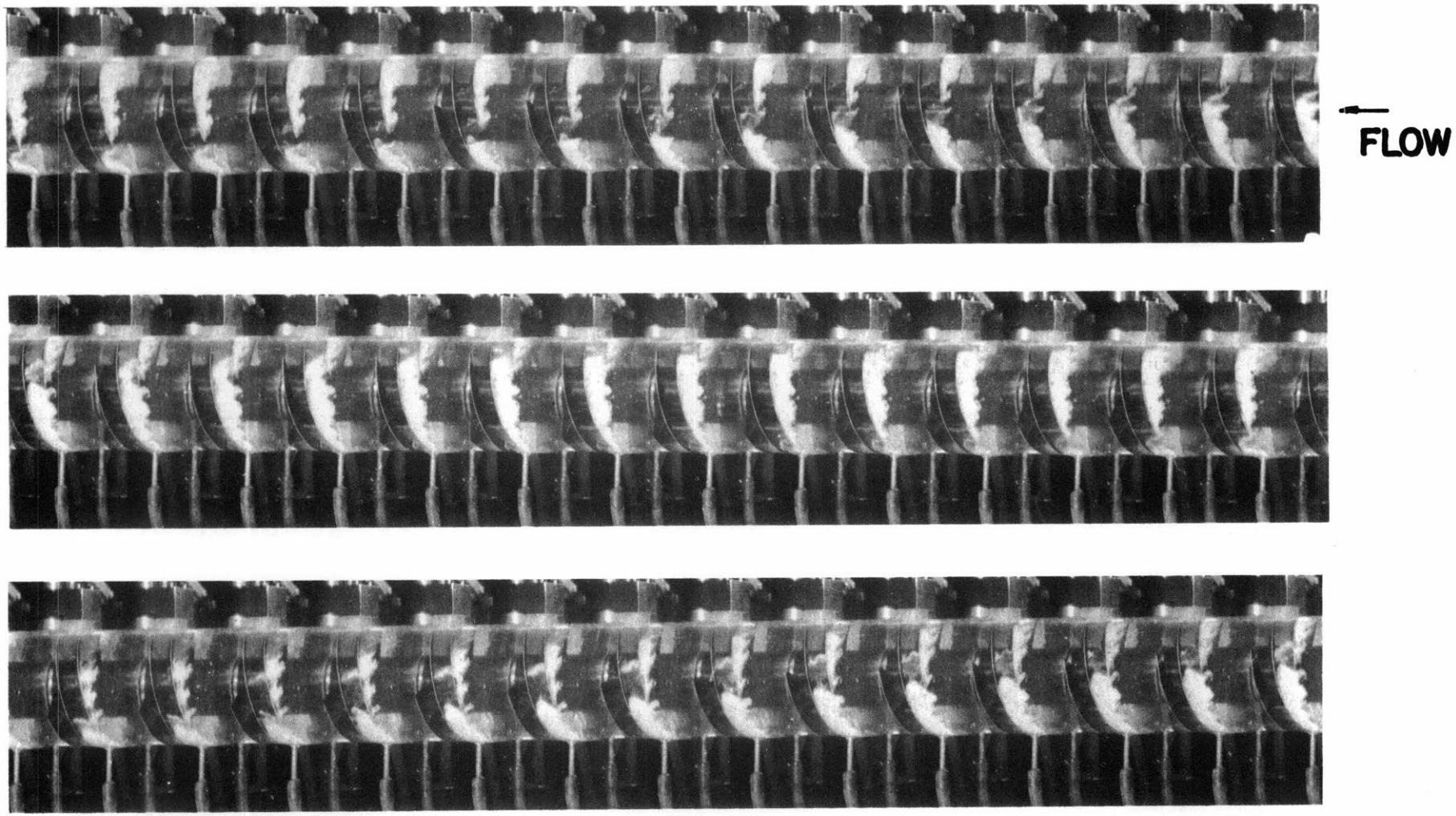

$\Phi = 0.126$, $K = 0.16$, 9,450 RPM

FIG. 30A - CAVITATION FORMATION (F.P. INDUCER)

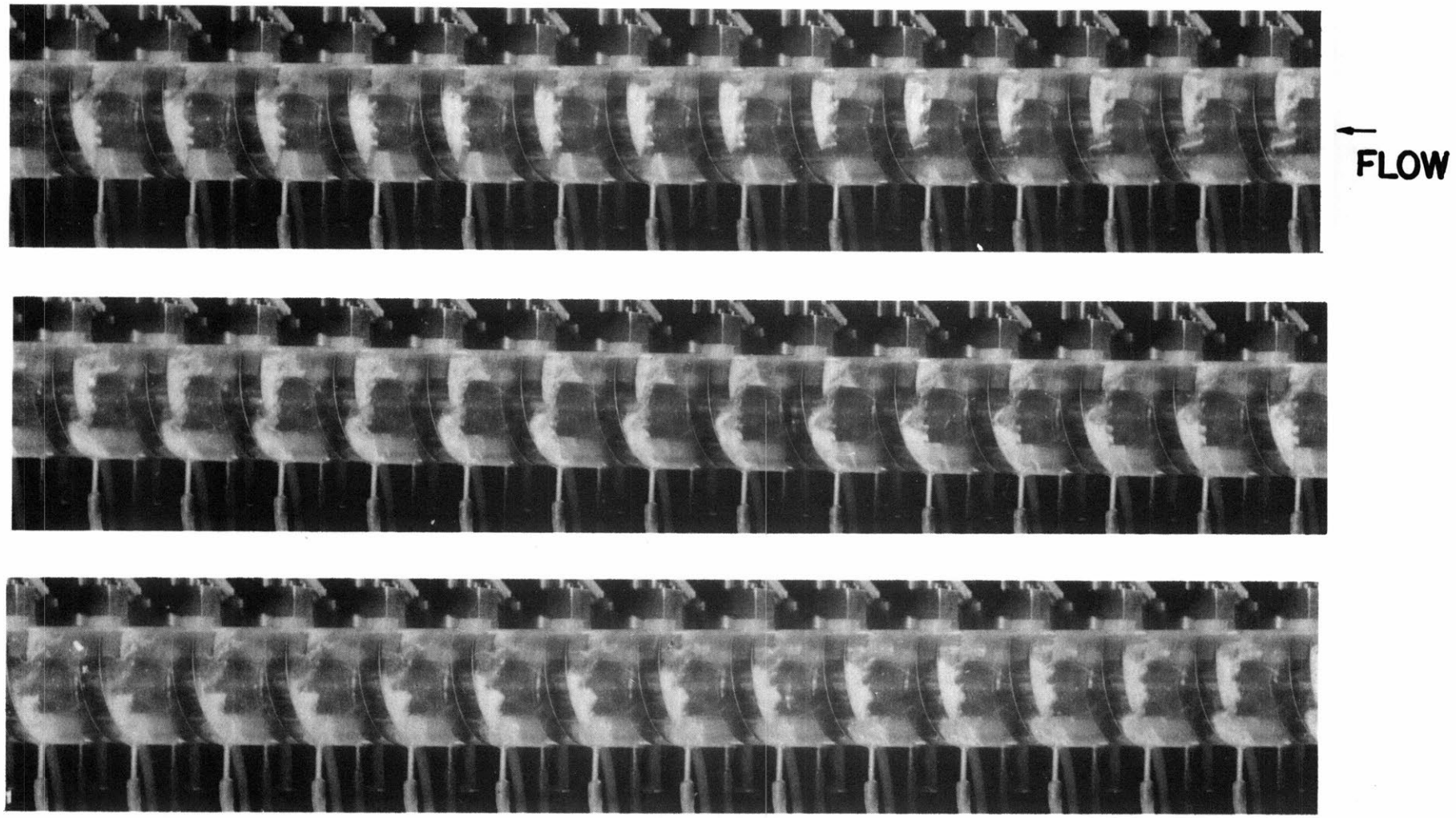

$\Phi = 0.126$, $K = 0.098$, 9,450 RPM

FIG. 30B- CAVITATION FORMATION

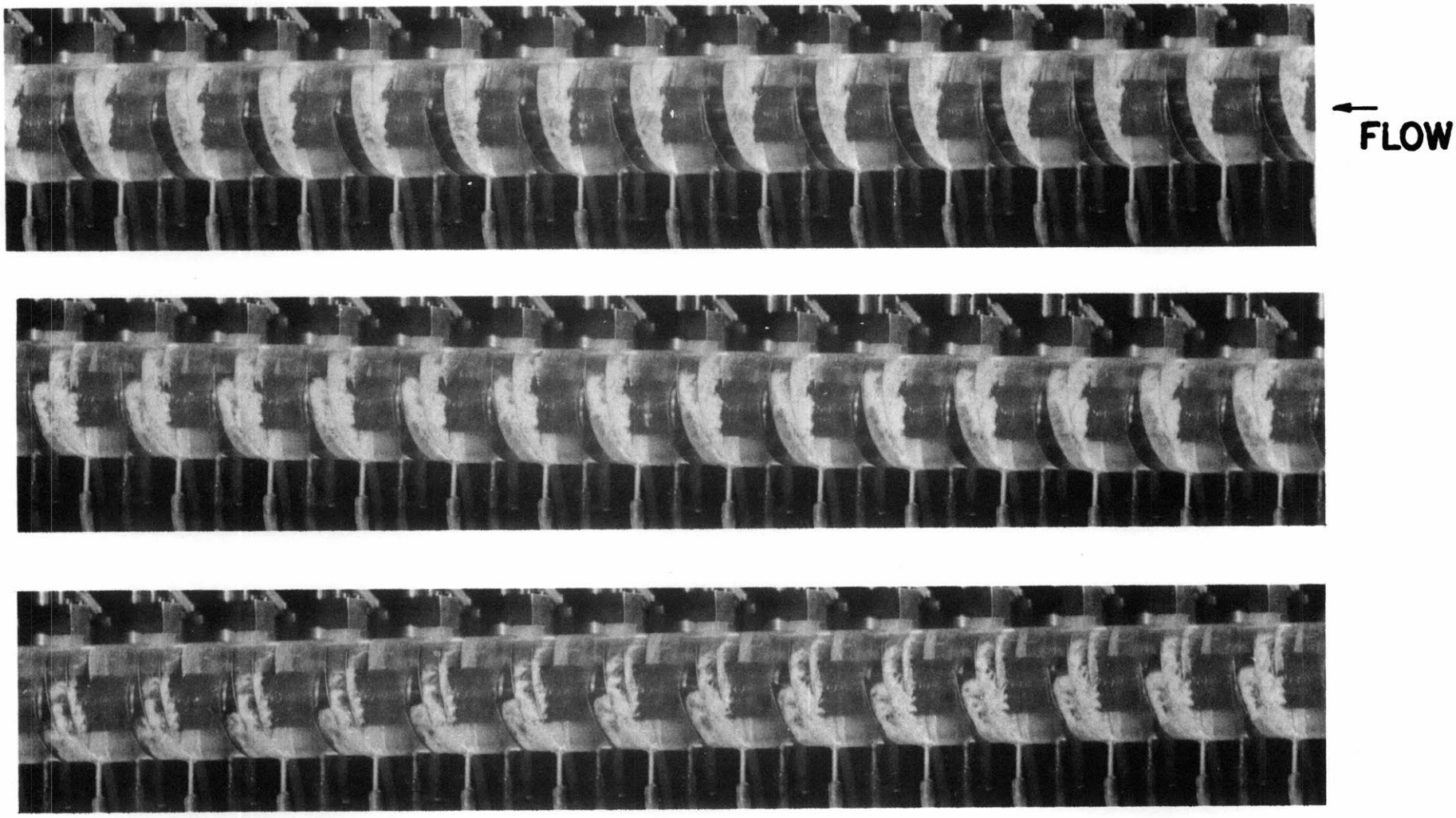

$\Phi = 0.126$, $K = 0.064$, 9,450 RPM

FIG. 30C- CAVITATION FORMATION

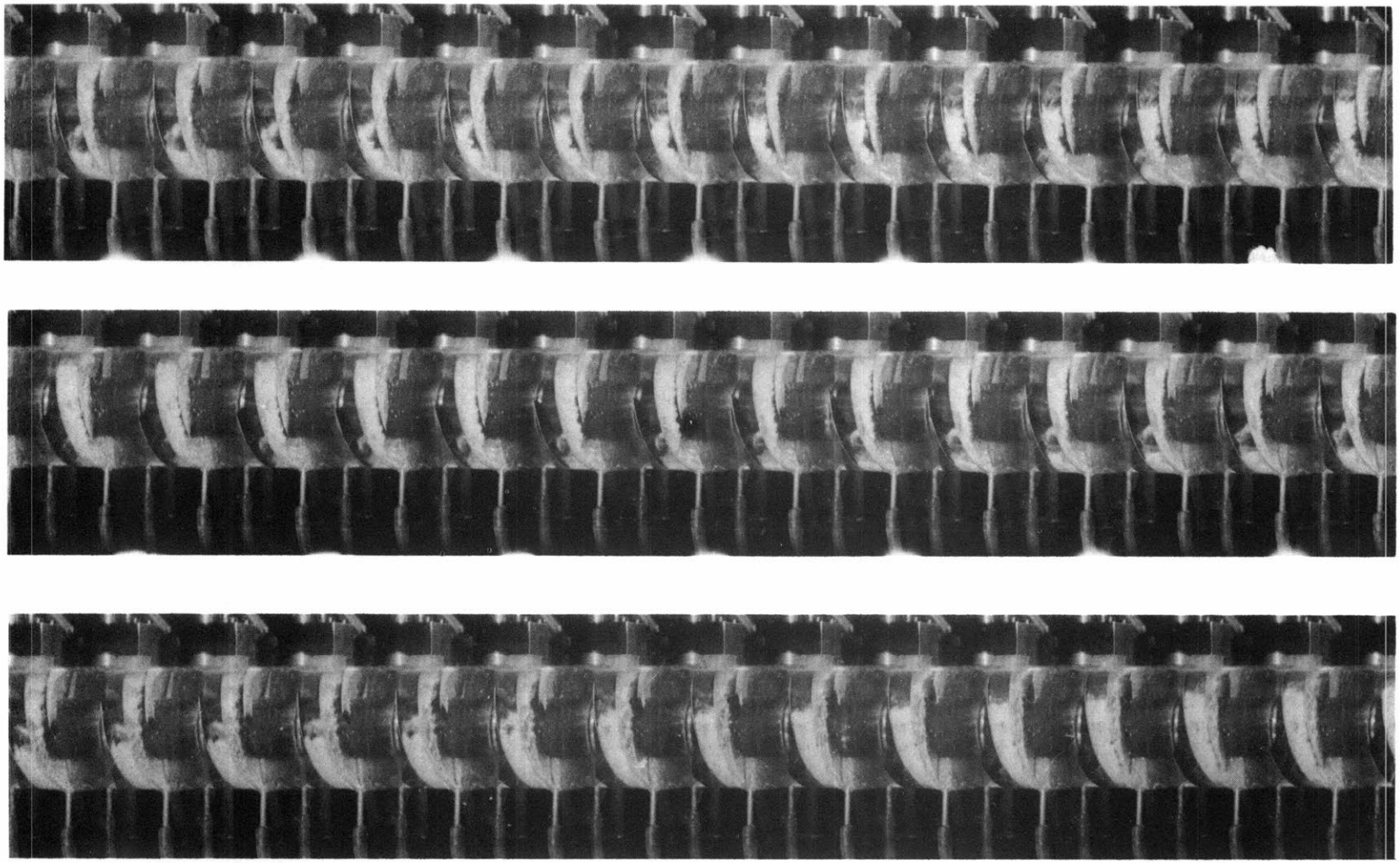

$\Phi = 0.126$, $K = 0.034$, 9,450 RPM

FIG. 30D - CAVITATION FORMATION

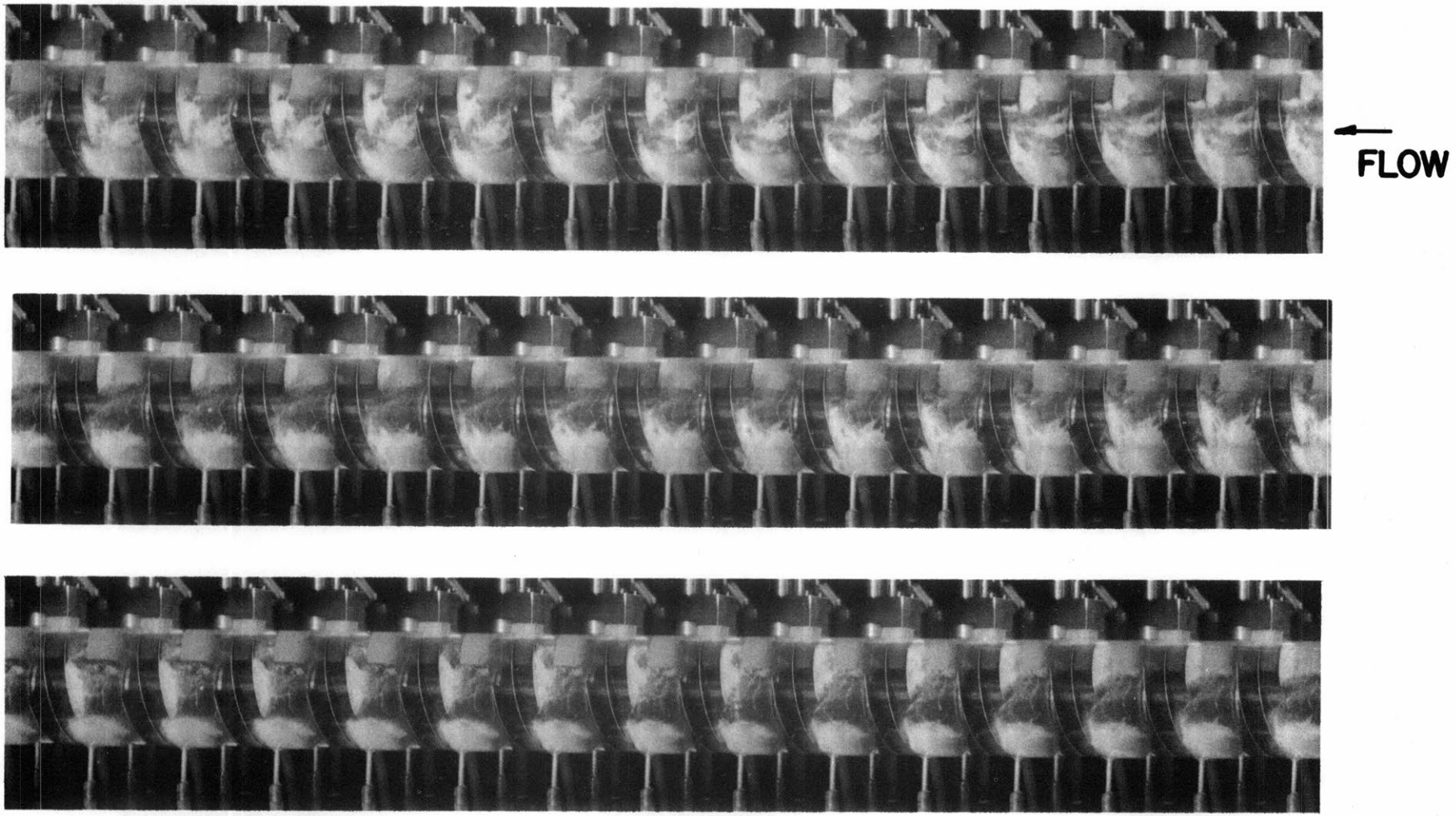

$\Phi = 0.10$, $K = 0.14$, 9,100 RPM

FIG. 31A- CAVITATION FORMATION (F. P. INDUCER)

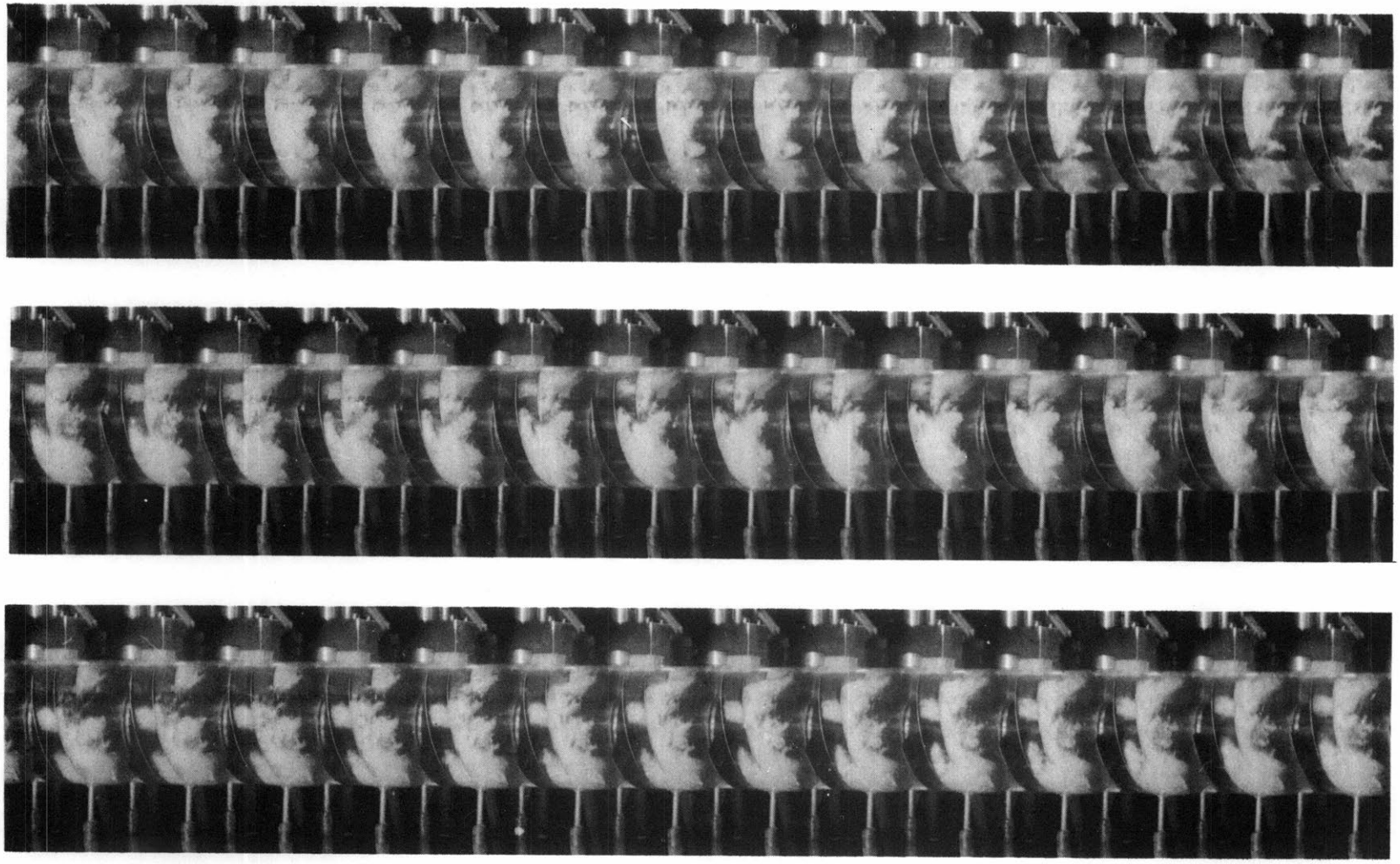

$\Phi = 0.10$, $K = 0.08$, 9,100 RPM

FIG. 31B - CAVITATION FORMATION

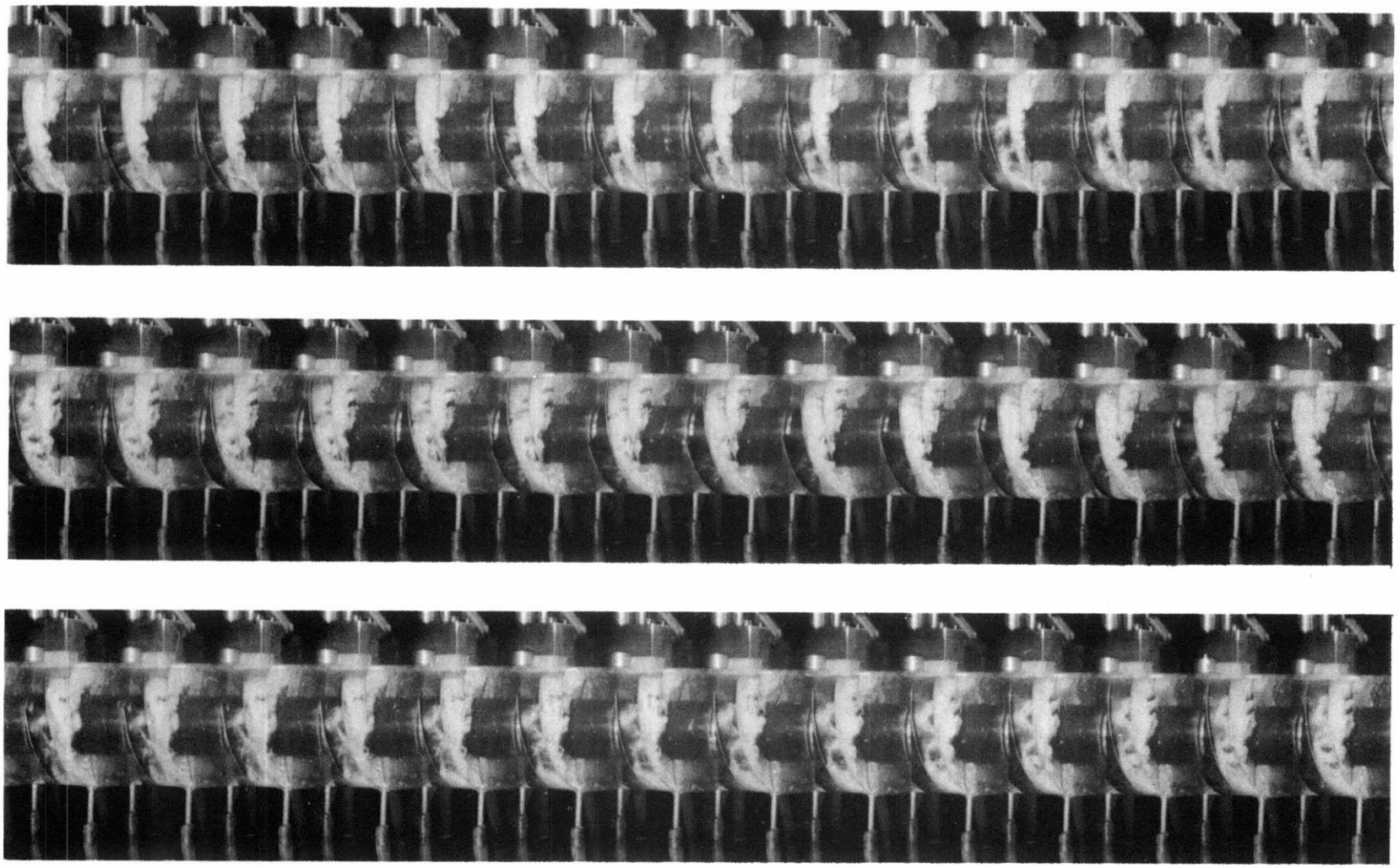

Φ=0.10, K=0.036, 9,100RPM

FIG. 31C - CAVITATION FORMATION